scientific reports

Check for updates

OPEN

ERG1A K^+ channel increases intracellular calcium concentration through modulation of calsequestrin1 in C_2C_{12} myotubes

Gregory H. Hockerman[1,7], Evan Pratt[1,7], Shalini Guha[2], Emily LaVigne[1], Clayton Whitmore[2], Omar Khader[2], Natalie McClure[2], Sandra Zampieri[3,4], Jennifer Koran[5], W.-H. Wang[6] & Amber L. Pond[2]✉

The ERG1A K^+ channel modulates the protein degradation that contributes to skeletal muscle atrophy by increasing intracellular calcium concentration ($[Ca^{2+}]i$) and enhancing calpain activity, but the mechanism by which the channel regulates the $[Ca^{2+}]i$ is not known. Here, we have investigated the effect of human ERG1A (HERG) on $[Ca^{2+}]i$ in C_2C_{12} myotubes, using Fura-2 calcium assays, immunoblot, RT-qPCR, and electrophysiology. The data show that the rise in $[Ca^{2+}]_i$ induced by KCl-stimulated depolarization is of greater amplitude in C_2C_{12} myotubes over-expressing HERG relative to controls, but this difference does not result from an increase in L-type channel ($Ca_v1.1$) Ca^{2+} influx because there is no statistical difference in the nifedipine-sensitive response upon depolarization between the expression groups. Indeed, HERG overexpression in C_2C_{12} myotubes has no effect on the amplitude of L-type channel current nor does it affect the mRNA levels nor protein abundance of the Cav1.1 channel. This finding suggests that HERG modulates excitation coupled calcium entry (ECCE). Indeed, the HERG-enhanced increase in $[Ca^{2+}]i$ induced by depolarization is blocked by 2-aminoethoxydiphenyl borate, an inhibitor of ECCE. Further, HERG also modulates the activity of ryanodine receptors (RYR1, a component of ECCE) as well as store operated calcium entry (SOCE). Therefore, we investigated the effect of HERG on calsequestrin1, a calcium buffering/binding protein known to modulate RYR1 and SOCE activities. Indeed, we find that calsequestrin1 mRNA levels are decreased 0.83-fold ($p < 0.05$) and the total protein abundance is lowered 77% ($p < 0.05$) in myotubes over-expressing HERG relative to controls. In conclusion, the data show that ERG1A overexpression modulates $[Ca^{2+}]i$ in skeletal muscle cells by lowering the abundance of the calcium buffering/binding protein calsequestrin1 which interacts with RyR1 and SOCE pathways. Indeed, we report that overexpression of HERG in myotubes increases $[Ca^{2+}]_i$ by modulation of RyR1 as well as ECCE and SOCE activities. It is likely that HERG enhancement of RyR1 activity, through decreased Casq1 abundance, is increasing $[Ca^{2+}]i$. This study provides a potential mechanism to explain how upregulation of ERG1A contributes to increased $[Ca^{2+}]i$ and, thus, atrophy in skeletal muscle.

Keywords Ether-a-gogo related K^+ channel, Skeletal muscle, Intracellular calcium, RyR1, Store operated calcium entry, calsequestrin1

Abbreviations

2-APB	2-Aminoethoxydiphenyl borate
ANOVA	Analysis of variance
AUC	Area under the curve

[1]Medicinal Chemistry and Molecular Pharmacology Department, Purdue University School of Pharmacy, West Lafayette, IN 47906, USA. [2]Anatomy Department, School of Medicine, Southern Illinois University, Life Sciences Building III, Room 2080, 1135 Lincoln Drive, Mail Code 6523, Carbondale, IL 62902, USA. [3]Department of Surgery, Oncology and Gastroenterology, University of Padova, Padua, Italy. [4]Department of Biomedical Sciences, University of Padova, Padua, Italy. [5]School of Education, SIU Carbondale, Carbondale, IL, USA. [6]Genetic Editing Core Facility, Purdue University, West Lafayette, IN, USA. [7]Gregory H. Hockerman and Evan Pratt contributed equally to the manuscript. ✉email: apond@siumed.edu

$[Ca^{2+}]i$	Intracellular calcium concentration
Casq1	Calsequestrin 1
CEU	Calcium entry units
df	Degrees of freedom
DHPR	Dihydropyridine receptor
DMEM	Dubelco's minimum essential medium
ECC	Excitation contraction coupling
ECCE	Excitation coupled calcium entry
ERG1	Ether-a-gogo related gene 1
FBS	Fetal bovine serum
GFP	Green fluorescent protein
HERG	Human ERG1
HS	Horse serum
IP_3R	Inositol triphosphate receptor
KRBH	Krebs–Ringer buffer with HEPES
MERG	Mouse ERG1
mKRBH	Modified Krebs–Ringer buffer with HEPES
MOI	Multiplicity of infection
No RT	No reverse transcriptase added control
NTC	No template control
OD	Optical density
PBS	Phosphate buffered saline
rtPCR	Real time polymerase chain reaction
RyR1	Ryanodine receptor 1
SD	Standard deviation
SDB	Sample diluting buffer
SDS-PAGE	Sodium dodecyl sulfate-polyacrylamide gel electrophoresis
SEMD	Standard error of the mean difference
SERCA	Sarcoendoplasmic reticulum Ca^{2+}-ATPase
SOCE	Store operated calcium entry
SR	Sarcoplasmic reticulum
Tg	Thapsigargin
TTBS	Tris-buffered saline with 0.1% tween-20, 5% NGS and 0.1% sodium-azide
UPP	Ubiquitin proteasome proteolysis

Background

The *ether-a-go-go related gene* (*erg1*) encodes a number of ERG1 K^+ channel alpha subunit alternative splice variants. Two ERG1 splice variants, which have been cloned from both human ERG1 (HERG1A and 1B;[1]) and mouse *Erg1* (*Merg1a* and *1b*;[2]) cDNA libraries, form a heteromultimeric channel in mammalian heart. This ERG1A/1B channel has been shown to produce $I_{Kr,}$ a current which is partially responsible for late phase repolarization of the cardiac action potential[3,4]. We have shown that the ERG1A K^+ channel subunit contributes to skeletal muscle loss in atrophic situations through up-regulation of ubiquitin proteasome proteolysis (UPP); we do not detect ERG1B in skeletal muscle[5]. Specifically, our labs have reported that the ERG1A K^+ channel is up-regulated in skeletal muscle of mice undergoing atrophy as a result of hind limb unweighting[5], tumor-induced cachexia[5,6], and denervation[7]. Moreover, we have reported that: (1) pharmacological and genetic block of ERG1A function inhibit skeletal muscle atrophy induced by hind limb suspension[5], (2) atrophy is induced in mouse muscle by ectopic expression of wild type *Erg1a*[5]; and (3) abundance of the UPP E3 ubiquitin ligase MuRF1 (but not ATROGIN1) and overall UPP activity are increased in mouse skeletal muscle by ectopic overexpression of *Erg1a*[5,8,9]. Further, we have shown that the ERG1A K^+ channel protein is expressed at low abundance in C_2C_{12} myotubes and that augmentation of its expression in these cells, as in mouse skeletal muscle, will induce a decrease in cell size (i.e., myotube area) and an increase in the abundance of the E3 ubiquitin ligase MuRF1, but not the E3 ligase ATROGIN1[10]. Finally, human Erg1A (HERG) overexpression in C_2C_{12} myotubes induces a significant increase in basal intracellular calcium ($[Ca^{2+}]i$) and calpain activity at 48 h after transduction[10]. Thus, upregulation of ERG1A contributes to skeletal muscle atrophy in vivo, and ectopic expression of HERG in C_2C_{12} myotubes induces an atrophic phenotype in vitro. Given the potentially important role of Ca^{2+} in modulation of skeletal muscle health and atrophy, we sought to understand the mechanism whereby HERG expression elevates basal $[Ca^{2+}]i$ in C_2C_{12} myotubes[10].

Intracellular Ca^{2+} is essential for excitation–contraction coupling (ECC) in skeletal muscle. Specifically, Cav1.1 L-type voltage-gated Ca^{2+} channels (also known as dihydropyridine receptors, DHPR) are activated by the depolarizing action potentials that spread longitudinally along the muscle sarcolemma and inwardly into the myofibers along the t-tubules, where they are juxtaposed to ryanodine receptors 1 (RyR1). Through a physical interaction, the RyR1 and Cav1.1 together allow release of Ca^{2+} from the sarcoplasmic reticulum (SR) into the cytosol through the RyR1 channel. This increase in $[Ca^{2+}]i$ (μM range) triggers skeletal muscle contraction, which is reversed when Ca^{2+} is "pumped" back into the SR by sarcoendoplasmic reticulum Ca^{2+}-ATPase (SERCA) (reviewed in Cho et. al.[11]). Smaller increases in $[Ca^{2+}]i$ (nM range) also occur in cells and these modulate muscle cell events such as upregulation of muscle thermogenesis in non-contracting muscle in response to cold[12] and increase of both fatigue resistance and mitochondrial biogenesis[13]. Localized Ca^{2+} concentration fluctuations also serve as second messengers, modulating numerous signaling systems[14]. Thus,

$[Ca^{2+}]i$ is affected by mechanisms other than the physical interaction between Cav1.1 and RyR1 that occurs in response to sarcolemmal membrane depolarization (i.e., ECC). One mode of Ca^{2+} modulation which results in relatively small changes in $[Ca^{2+}]i$ is termed excitation coupled Ca^{2+} entry (ECCE). This Ca^{2+} influx is activated in response to prolonged and repetitive depolarization (e.g., by treatment with mM KCl in vitro) through a Cav1.1 and RyR1-mediated interaction, but it is insensitive to lower concentrations (≤ 10 μM) of the L-type current inhibiting reagent nifedipine[15,16]. It is inhibited by 2-APB, which also blocks store operated Ca^{2+} entry (SOCE) and IP3 receptors at the concentrations we used (100 μM), but is not affected by Ca^{2+} store depletion[17,18]. ECCE requires both RyR1 and Cav1.1 proteins[17] and L-type channel pore permeation appears to contribute to this calcium ion passage[15]; however, it is still likely that this extracellular entry mechanism may require another (as yet unidentified) sarcolemmal Ca^{2+} channel or other auxiliary units[19]. To date, it has been shown that Orai1[20] and TRPC3[21] are not candidates for this role. Calcium is also brought into the cell from the extracellular milieu through SOCE. SOCE is inhibited by depolarization and is activated by depletion of intracellular Ca^{2+} stores (i.e., the SR)[22]. Specifically, SR depletion results in dimerization of two SR membrane STIM1 proteins which are a major component of SOCE. Once dimerized, the STIM1 proteins then translocate through the SR membrane to interact with and open the sarcolemmal membrane Orai1 Ca^{2+} channel through which the Ca^{2+} moves into the cell from the extracellular milieu[23–25].

Here, we show that, relative to controls, the abundance of the Ca^{2+} buffering/binding protein calsequestrin1 (Casq1) is significantly lower in HERG over-expressing myotubes. Because RyR1 and SOCE activities are inhibited by Casq1 at higher concentrations of $[Ca^{2+}]i$[26–29], the down regulation of Casq1 in response to HERG overexpression could increase the concentration of free calcium in the SR, and produce an increase in Ca^{2+} outflow from SR stores when release is stimulated. Indeed, we observe that overexpression of HERG increases RyR1 activity. The activation of RyR1 could also potentially stimulate the ECCE, which would increase influx of calcium to the cytosol from the extracellular milieu. We do report here an increase in ECCE activity with HERG overexpression. Additionally, we note that HERG overexpression enhances SOCE activity, which may perhaps occur as a direct effect on a SOCE component or from the decrease in $[Ca^{2+}]_{SR}$ resulting from the HERG-related increased RyR1 activity. Indeed, we report here that the activities of RyR1 and the ECCE as well as the SOCE pathway are enhanced in myotubes over-expressing HERG.

Materials and methods

Cell culture

C_2C_{12} cells (ATCC; Manassas, VA) were cultured in Dulbecco's Minimum Essential Medium (DMEM; ThermoFisher Scientific; Waltham, MA) containing 25 mM glucose, 4 mM L-glutamine and 3.7 g/L sodium bicarbonate and supplemented with 10% fetal bovine serum (FBS; ThermoFisher Scientific) within a 37 °C incubator containing 6.5% CO_2. Differentiation of myoblasts into myotubes was induced by switching to culture medium as described here except that the 10% FBS was replaced with 2% heat-inactivated horse serum (HS). After replacement of medium, cells were allowed to differentiate for 7–8 days at which point myotubes were transduced and allowed to incubate another 48 h with virus (i.e., another 2 days to produce 9–10 days cultured cells).

Antibodies

All antibodies (except the antibodies used in Additional file 3) were diluted in phosphate buffered saline (PBS, pH 7.4) with 5% normal goat serum, 0.1% Triton X-100, and 0.01% sodium azide. For the Casq11 immunoblot in Fig. 8 (Panel B), the Calsequestrin1 D-10 (sc-137080; Santa Cruz, Dallas, TX) mouse monoclonal primary antibody was diluted in this buffer at 1:100. To detect Cav1.1 α1 protein, the DHPR α1 primary antibody (MA3-920; ThermoScientific) was used at a 1:500 dilution. For GAPDH protein immunoblots, we probed the membranes with a monoclonal antibody (Clone 6C5, MilliporeSigma; St. Louis, MO) diluted 1:8000 and the β-tubulin antibody (T8328, Sigma) was diluted 1:2000. The alkaline phosphatase conjugated goat anti-mouse IgG antibody (BioRad; Hercules, CA) was used as secondary antibody (with all of the primary antibodies described above) at 1:10,000 in blotting buffer (0.2% non-fat dry milk or casein and 0.1% Tween-20 in Tris Buffered Saline, pH 7.4; Sigma; St. Louis, MO). For the immunoblot in AD3, the Casq1-specific primary antibody 26665-1-AP (ProteinTech; Rosemont, IL) was diluted 1:1000 in 0.2% non-fat dry milk in Tris-buffered saline with 0.1% tween-20, 5% NGS and 0.1% sodium-azide (pH 7.4, TTBS) followed by washing in TTBS and then incubation in secondary antibody (goat anti-rabbit IgG-Alkaline Phosphatase; 65-6122 Sigma) diluted 1:1000 in 0.2% non-fat dry milk in TTBS.

Virus

The human ERG1A construct[30], was cloned into a viral cassette provided by ViraQuest, Inc. (North Liberty, IA) and then cloned by this company into the VQad CMV adenovirus (containing GFP expression apparati). The appropriate control virus was also purchased from this company and used for the control transfections. Both sets of viral particles were maintained at − 80 °C in small aliquots until used.

Viral transduction of C_2C_{12} myotubes

HERG and control viral particles were added to DMEM with 2% horse serum (Gibco/ThermoFisher; Waltham, MA) and mixed. This suspension was used to treat C_2C_{12} myotubes (cultured as described above) at 200 multiplicity of infection (MOI) as pre-determined by titration, EXCEPT that the myotubes used for the Casq1 and GAPDH immunoblots in Fig. 7 were treated with 400 MOI. The virus treated plates were gently agitated to properly disperse the viral particles and then returned to the incubator. Viral expression was monitored by GFP fluorescence and detected at 24 h post transfection; it appeared to plateau at 48 h, so this is when procedures were performed.

Intracellular calcium concentration assays

A Fura-2 QBT Calcium Kit (Molecular Devices; San Jose, CA) was used to assess $[Ca^{2+}]i$ according to manufacturer's instructions. Briefly, myotubes were grown in the wells of a 96-well plate as described earlier. The myotubes were then loaded with Fura-2 QBT by incubation with 1:1 Gibco Opti-MEM (Life Technologies; Carlsbad, CA) and Fura-2 QBT (dissolved at recommended concentration) in modified Krebs–Ringer Buffer with HEPES (mKRBH; 0.05% fatty acid free bovine serum albumin in 134 mM NaCl, 3.5 mM KCl, 1.2 mM K_2HPO_4, 0.5 mM $MgSO_4$, 1.5 mM $CaCl_2$, 5 mM $NaHCO_3$, 10 mM HEPES) for 1 h at room temperature (RT) in the dark. This medium was then replaced with Fura-2 QBT solution (in mKRBH) containing either a treatment (as described below) or vehicle (as control) and incubated at RT in the dark for 30 min. A Synergy Mx Microplate Reader (Biotek; Winooski, VT) was used in conjunction with Gen5 2.0 software (Biotek; https://www.agilent.com/en/support/biotek-software-releases) to excite the samples at 340 nm and 380 nm and to measure emission at 508 nm. The 340/380 nm emission ratio was determined for all recorded time points for each reaction (i.e., each assayed well of the plate). The 340/380 ratio of each well prior to addition of treatment represents the basal calcium levels. To normalize the data to the basal calcium levels, the average 340/380 ratio was determined for each well for all time points measured prior to addition of treatment and that result was subtracted from the 340/380 ratio for each time point recorded for that well after addition of treatment. The normalization to basal calcium levels *(recorded prior to addition of treatment)* is necessary to correct for the significant differences in basal $[Ca^{2+}]i$ levels between control and HERG-over-expressing myotubes. Indeed, we have recorded/reported significantly higher $[Ca^{2+}]i$ levels in HERG over-expressing versus control myotubes at 48 h post transduction[10], the time at which we performed our Fura2 assays here to ensure HERG overexpression.

Depolarization assays

Myotubes were cultured and treated with either control virus or virus encoding HERG as described earlier. At 48 h post viral transduction, these myotubes were loaded with Fura-2 QBT and then treated with either vehicle or drug for 30 min. The drug was either: nicardipine (10 μM, an L-type Ca^{2+} current inhibitor), nifedipine (10 μM, an L-type Ca^{2+} current inhibitor), thapsigargin (Tg, 1 μM, an inhibitor of SERCA1), 2-aminoethoxydiphenyl borate (2-APB, Sigma; 100 μM to block SOCE, ECCE, and inositol triphosphate receptors [IP_3R]), or astemizole (Sigma; 1 nM, to block HERG channels). The fluorescence assay for $[Ca^{2+}]i$ (as described above) was monitored for one minute (to determine background) and then the cells were depolarized by addition of 100 mM KCl and assayed for an additional 2.5 min (in the continued presence of the KCl).

Ryanodine receptor activation assays

Myotubes were cultured and treated with either control virus or virus encoding HERG as described earlier. At 48 h post viral transduction, the myotubes were loaded with Fura-2 QBT and then treated for 30 min with ryanodine (100 μM, as determined by a dose–response curve to completely block caffeine induced Ca^{2+} release) to block RyR1. The Fura-2 QBT $[Ca^{2+}]i$ assay (as described above) was started for one minute and then the cells were treated with caffeine (10 mM) to activate RyR1 and finally assayed for an additional 1.5 min.

SOCE assays

Myotubes were cultured and transduced with either control adenovirus or adenovirus encoding HERG (as described above). At 48 h post viral transduction, the myotubes were loaded with Fura-2 QBT using mKRBH with 1.5 mM $CaCl_2$ (as described above). After 1 h, this buffer was removed and replicate wells of these cells (both control and HERG over-expressing) were then treated with calcium-free mKRBH (1.5 mM $MgCl_2$ replaced 1.5 mM $CaCl_2$) containing either vehicle or 2-APB (100 μM in vehicle to block SOCE activity) for 30 min. The cells were then assayed for $[Ca^{2+}]i$ as described above (340 and 380 nm wavelengths were monitored). Fluorescence was monitored for 1 min to establish a baseline. Then Tg (1 μM) was dispensed into all wells to "empty" the SR stores and fluorescence measurement was continued for an additional 20 min at which time $CaCl_2$ (2.5 mM final) was added to activate SOCE. Fluorescence assay was continued for an additional 10 min. To evaluate the data, the 340/380 ratios were determined. First, to ascertain the effect of the Tg only, we analyzed the data by subtracting the average ratio of the first minute time points (baseline) from the ratios of each time point measured from Tg addition until calcium was added. We noted that the "baselines" prior to addition of calcium for each 2-APB treated sample were statistically different from the paired samples not treated with 2-APB. Therefore, we normalized the post calcium addition data (i.e., SOCE activity) to the average "baseline" calculated for two minutes prior to addition of calcium. That is, the 340/380 nm ratio measured in each well at each time point for two minutes prior to the addition of calcium was averaged and subtracted from the 340/380 nm ratio for each time point after addition of $CaCl_2$ to normalize data to background as an assessment of $[Ca^{2+}]i$ flux. This normalization was done to correct for differences (i.e., increases) in basal calcium levels that occur in response to HERG overexpression during Tg incubation. We also normalized these data to the average 1-min baseline for comparison.

RNA isolation and RT-qPCR

Total RNA was extracted from control and HERG-expressing C_2C_{12} myotubes using Trizol reagent (Life Technologies; Carlsbad, CA) according to manufacturer's instructions followed by chloroform solubilization and ethanol precipitation. RT-qPCR (quantitative reverse transcriptase PCR) was then performed using a Luna® Universal One-Step RT-qPCR Kit (New England Biolabs; E3005) per manufacturer's instructions and primers for the Casq1 gene of interest (IDT; San Jose, CA) along with primers for ERG1A (Invitrogen; Waltham, MA) and the GAPDH "housekeeping gene" (IDT) (Table 1). A CFX BioRad OPUS 96 real time PCR system (BioRad; Carlsbad, CA) was used to detect SYBR green fluorescence as a measure of amplicon. Changes in gene expression were determined using the Livak method to normalize the gene of interest to the "housekeeping

	Primer sequence 5′–3′	Size (bp)	Tm (°C)	GC (%)	Amplicon size (bp)
Merg1a forward	cctcgacaccatcatccgca	20	59.6	55.0	145
Merg1a reverse	aggaaatcgcaggtgcaggg	20	60.3	60.0	
Calsequestrin1 forward	atgagagctaccgacaggatg	21	56.3	55	105
Calsequestrin1 reverse	caccgtcgtactcagggaag	20	54.4	50	
GAPDH forward	actcccactcttccaccttc	20	56.3	55	272
GAPDH reverse	ctaggcccctcctgttattatg	22	54.4	50	

Table 1. Primer sequences for RT-qPCR. *bp* base pairs.

gene." No template controls (NTC) and no-reverse transcriptase (no-RT) controls were also assayed along with our samples of interest in each set of PCR reactions to assess and ensure assay quality.

Cell lysate preparation and protein assay

C_2C_{12} cells were differentiated in 10 cm plates for 7–8 days and then transduced with either control or HERG-encoded virus and incubated an additional 48 h. Membrane proteins were extracted from myotubes by gently washing tissue culture plates twice with room temperature PBS and then scraping cells from the plates treated with 200 µL of cold Tris–EDTA buffer (10 mM, 1 mM respectively, pH 7.3; Sigma) containing 2% Triton-X100 (Sigma) and protease inhibitors: 0.5 mM pefabloc, 1 mM benzamidine, 1 mM iodoacetamide, 1 mM 1,10-phenanthroline, and a commercial protease cocktail tablet (Pierce A32955 [ThermoFisher] used per manufacturer instructions). Cell suspensions were homogenized on ice with a 27.5-gauge needle and 1 mL syringe (~30 s) and then again with a 30.5-gauge needle and 1 mL syringe (~30 s). The samples were then allowed to sit within ice in a refrigerator for 20 min to enhance membrane solubilization. The cell lysates were then passed through an Eppendorf pipette (200 uL tip) multiple times and centrifuged at 12,000×*g* for 10 min to remove solid material. Sample supernatants were collected and stored at − 80 °C.

Protein determination

To determine sample protein concentration, a standard curve was developed using BSA (Sigma) and then a DC Protein Assay kit (BioRad; Carlsbad, CA) was used to develop color in the standards and samples from which protein content was determined by linear regression using Excel (Microsoft 365; Redmond, WA; https://www.microsoft.com/).

Immunoblot

For immunoblots, aliquots of equal protein content (40 ug, except Additional file 3C,E) were boiled for 5 min after dilution in sample buffer (5X SDB; 0.3 M Tris [pH 6.9], 50% glycerol, 5% SDS, 0.5 M dithiothreitol, and 0.2% bromophenol blue). Samples were then electrophoresed through a 4–20% polyacrylamide (SDS-PAGE) gradient gel, transferred to PVDF membrane (BioRad; Hercules, CA), and immunoblotted using antibodies specific for either: Casq1, Cav1.1 (also called DHPR), GAPDH, or β-tubulin. Secondary antibodies conjugated with alkaline phosphatase were used with an ImmunStar™-Alkaline Phosphatase (AP) Western Chemiluminescent Kit (Bio-Rad) for signal development. To ensure that lanes were loaded equally, after development for Casq1 or Cav1.1 signal, PVDF membranes were incubated (30 min at room temperature) in stripping buffer (62.5 mM Tris Cl [pH 6.9], 2% SDS, 0.695% BME in water), rinsed with 0.1% Tween 20 in 20 mM Tris (TTBS, pH 7.4) and re-probed with GAPDH or β-tubulin antibody (see next section for imaging details). To further confirm protein loading equity, Coomassie Blue stain solution (0.1% Coomassie Blue R-250 in 45% methanol and 10% acetic acid in water) was used to stain the membranes overnight, after which these were destained with 50% methanol and 10% acetic acid in water.

Immunoblot imaging

ImageJ (NIH; Version 1.51 23 April 2018; https://imagej.net/ij/) was used to determine the optical densities of the protein bands: a single region of interest (ROI) which encompassed each protein band was outlined and this ROI was used to demarcate each protein band and a background area above each band. The average uncalibrated optical density (OD) was determined for each ROI and the background OD was subtracted from the OD of each target protein band (e.g., Cav1.1 and Casq1). The same was done for the internal reference protein. Then to correct for any differences in sample loading, for each sample a ratio was calculated by dividing the background-corrected OD for each target protein by the background-corrected OD for the "housekeeping protein" for each sample.

Electrophyisology: barium current densities

C_2C_{12} myoblasts were seeded in 35 mm cell culture dishes, differentiated to myotubes, and transduced with either control eGFP encoded virus or HERG encoded virus as described. Micropipettes were pulled from borosilicate capillaries to an inside diameter of 3–5 microns using a Sutter P-87 pipette puller, and polished with a Narishige MF 830 microforge. The pipette solution contained (mM): 180 N-methyl-D-glucamine, 40 HEPES, 4 $MgCl_2$, 12 phosphocreatine, 5 BAPTA, 2 Na_2ATP, 0.5 Na_3GTP, 0.1 leupeptin, and pH was adjusted to 7.3. The extracellular solution contained (mM): 140 NaCl, 20 $CsCl_2$, 10 $BaCl_2$, 10 HEPES, 10 glucose, 10 sucrose, 1 $MgCl_2$, and pH was adjusted to 7.4. Voltage clamp data were acquired with Clampex version 10.7.03, and analyzed with

Clampfit version 10.7.03 (Molecular Devices; https://www.moleculardevices.com/products/axon-patch-clamp-system). Voltage dependent barium currents were measured under voltage clamp using an Axopatch 200B amplifier (Axon Instruments). Data were sampled at 10 kHz and filtered at 1 kHz. Cells were held at − 80 mV and stepped to test voltages ranging from − 60 mV to + 50 mV in 10 mV increments. Current densities (pA/pF) were calculated by dividing the largest current amplitude for each cell, regardless of test voltage, by the whole cell capacitance. Diagrams depicting voltage clamp data in Fig. 2 were produced using SigmaPlot 11.0 (Systat Software; https://systatsoftware.com).

Statistics

All calculations, statistical analyses, and graphics (except those in Fig. 2) were accomplished using GraphPad Prism 9 (Dotmatics; Boston, MA; https://www.graphpad.com/scientific-software). A Student's T-test was used to analyze the optical density data from the immunoblots, the Ca^{2+} current densities, and the HERG and Casq1 gene expression data. A one-way ANOVA was used to analyze the AUC data from the RyR1 and SOCE activity studies as well as the fold changes in Cav1.1 gene expression data. When significant differences were found, means were separated by Tukey's test. A 2 × 3 ANOVA was used to compare drug effects on $[Ca^{2+}]i$ in response to viral treatment (HERG or control). For the samples depolarized with KCl, the AUCs per time unit were determined and analyzed with a two-way ANOVA design for repeated measures and the interaction between HERG and treatment was examined for statistical significance. The percent change in AUCs resulting from 2-APB within cell expression group (control or HERG) were calculated by subtracting all 2-APB treated replicates from all non-treated replicates within a cell expression group and then compared between expression group (control versus HERG) using a Student's t-test. The drug-sensitive fluorescence values are represented by the mean difference between the control and drug-blocked samples. These were determined by subtracting the mean 340/380 ratio of the drug-blocked samples from the mean 340/380 ratio of the control sample for each timepoint. The standard error of the mean difference (SEMD) was calculated using Eq. 1:

$$SEMD = \sqrt{variance * \left(\frac{1}{n1} + \frac{1}{n2}\right)} \tag{1}$$

where

$$variance = \frac{\left[df1 * (SD1)^2\right] + \left[df2 * (SD2)^2\right]}{df1 + df2};$$

and n = sample number; df = n-1; SD is the standard deviation. The "1" and "2" labels (e.g., df1, df2, SD1, SD2, etc.) are sample designations (e.g., "1" = activated sample value and "2" = blocked-activated sample value).

The mean difference and SEMD were used to estimate *p* values using a comparison of means calculator[31].

Results

The HERG channel affects $[Ca^{2+}]i$ by modulation of excitation coupled calcium entry

Depolarization with KCl. HERG-expressing myotubes ([10] validates this viral expression model; also see Additional file 1) show a significantly higher intracellular Ca^{2+} concentration than control cells for ~ 1.5 min after depolarization with 100 mM KCl (Fig. 1A,B). *Nifedipine Block.* A 10 µM concentration of nifedipine was used to block L-type channel conductance. As reported by Bannister et al.[15], nifedipine will not block ECCE activity significantly until 50 µM. Here we show that nifedipine (10 µM) has a strong blocking effect on the increase in $[Ca^{2+}]i$ that normally occurs in response to depolarization in the control cells, inhibiting ~ 67.5% of the rise in $[Ca^{2+}]i$ at 20 s and then lowering it substantially (over 90% blocked) from 40 to 120 s (Fig. 1C,D). This demonstrates that a large portion of the increase in $[Ca^{2+}]i$, which occurs in control C_2C_{12} myotubes in response to depolarization, is a result of L-type channel activation. Nifedipine also has a strong effect on the rise in $[Ca^{2+}]i$ that occurs in response to depolarization in the HERG-expressing myotubes (Fig. 1D,E). It blocks approximately 60, 73, and 77% of the Ca^{2+} increase that occurs initially (at 20, 30, and 40 s, respectively; $p < 0.05$) and then ranges from 70 to 42% from 50 to 120 s. Although the nifedipine block does not appear as strong over time in the HERG-expressing cells, indeed, when the specific nifedipine-sensitive Ca^{2+} transients are determined and compared (Fig. 1F), there is no statistical difference in the initial nifedipine-sensitive response of the HERG-treated and control myotubes and virtually no difference beyond the initial ~ 10 s post depolarization. Thus, although HERG is inducing a greater increase in $[Ca^{2+}]i$ in response to depolarization, this effect does not appear to be the result of increased Cav1.1 activity at 48 h after transduction. We explored potential L-type channel involvement further. *L-Type Current Density.* Myotubes were transduced with either a HERG-encoded or an appropriate control virus and after 48 h were evaluated for L-type current using whole-cell voltage clamp of myotubes (see Methods). The data demonstrate that HERG had no effect on peak L-type channel Ba^{2+} current density (Fig. 2 A,B) except at only the two most positive voltages (Fig. 2C). *Skeletal Muscle L-Type Channel Gene Expression.* Control and HERG-expressing myotubes were assayed for expression of genes encoding Cav1.1, embryonic Cav1.1 (Cav1.1e), Cav1.2, and Cav1.3 using RT-qPCR. No significant differences were found in expression of genes encoding Cav1.1 or Cav1.1e at 0, 48, or 60 h after transduction (Fig. 3 A,B). Expression of genes encoding Cav1.2 and 1.3 was not detected at these time points in either control or HERG-expressing myotubes. *Skeletal Muscle L-Type Channel α Subunit Protein Abundance.* Lysates from control and HERG-expressing myotubes were immunoblotted (Fig. 3C; Additional File 2) using an antibody specific for the skeletal muscle Cav1.1 channel α subunit and protein signal was detected by chemiluminescence (see Methods). The ODs of the Cav1.1 protein band reveal that HERG had no effect on Cav1.1 protein abundance (Fig. 3D).

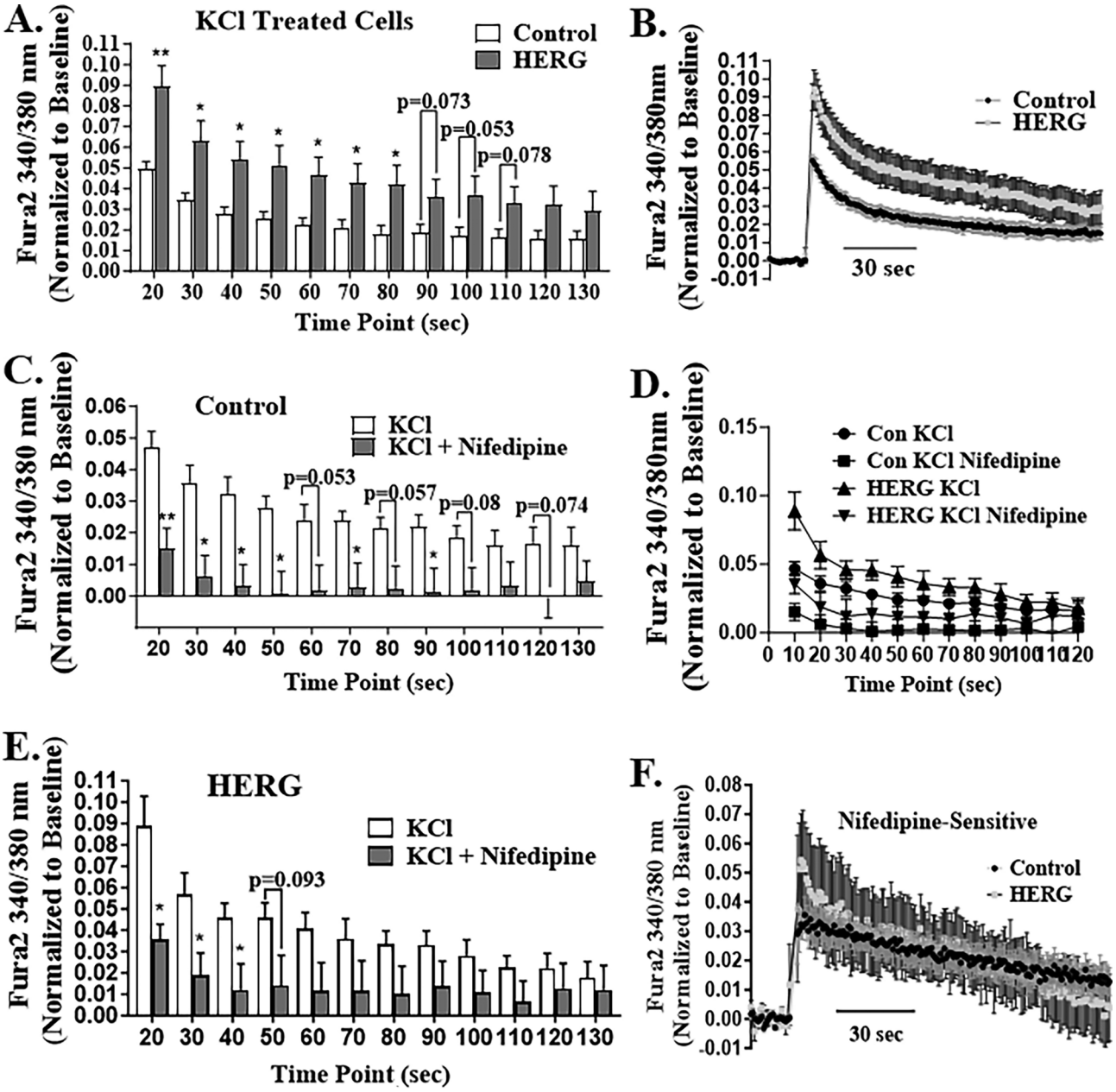

Fig. 1. HERG does not enhance intracellular calcium concentration ($[Ca^{2+}]i$) through modulation of the L-type channel in skeletal muscle. (**A**) The increase in intracellular Ca^{2+} ($[Ca^{2+}]i$) initiated by depolarization (with 100 mM KCl treatment) is significantly greater in myotubes expressing HERG relative to controls. (**B**) Change of $[Ca^{2+}]i$ in control and HERG treated cells in response to KCl treatment over time (cells from Figure **A**). (**C**) Nifedipine (10 μM) has a significant inhibitory effect on the increase in $[Ca^{2+}]i$ that occurs in control cells in response to depolarization over 90 s after addition of KCl. (**D**) Change of $[Ca^{2+}]i$ in control and HERG treated cells in response to KCl and nifedipine treatments over time (cells from Figure **C**). (**E**) Nifedipine also inhibits a portion of the HERG-induced increase in $[Ca^{2+}]i$ for up to 40 s. (**F**) Nifedipine-sensitive fluorescence ratios do not differ significantly between the control and HERG-expressing myotubes, demonstrating that the HERG-modulated increase in $[Ca^{2+}]i$ does not result from activation of L-type Ca^{2+} channels. $[Ca^{2+}]i$ was evaluated by the ratiometric fluorescent Fura-2 dye. The 340/380 nm ratios were determined, normalized to baseline, and analyzed by a 2 × 2 ANOVA design for repeated measures. There was no statistically significant interaction between HERG and treatment. The bars (**A**,**C**,**E**) and symbols (**B**,**D**,**F**) represent means. The error bars represent standard error of the mean. n = 16 (8 control and 8 HERG-expressing myotubes). $^{*}p < 0.05$, $^{**}p < 0.01$.

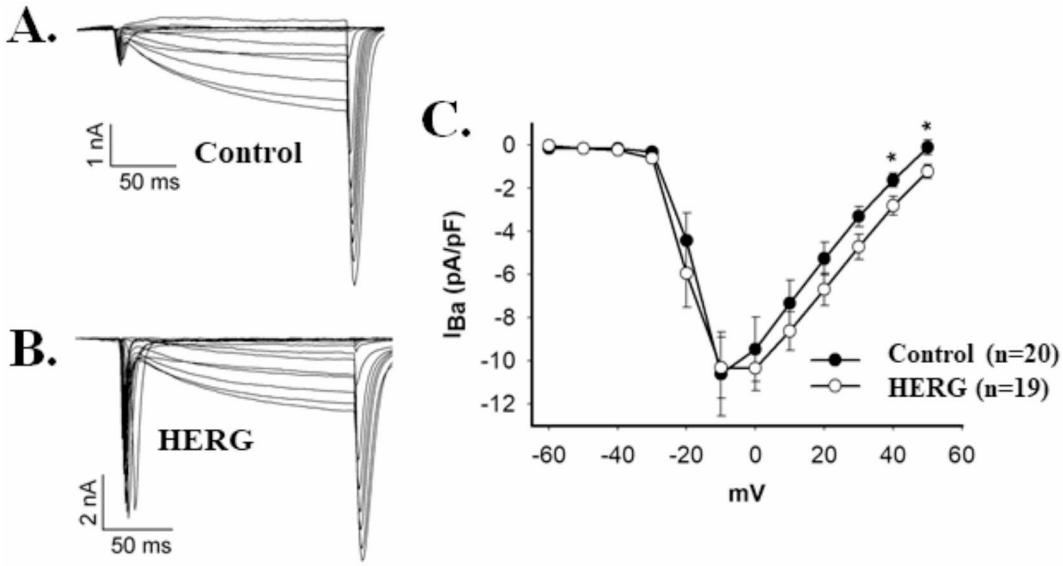

Fig. 2. HERG Expression does not change peak Cav channel current density in C_2C_{12} myotubes. (**A**,**B**) Example ensembles of current traces elicited by stepping from −80 mV to 50 mV in 10 mV increments for 150 ms, from a holding potential of −60 mV in a control transduced myotube (**A**) or a HERG transduced myotube (**B**). Currents in (**A**) and (**B**) were recorded in a bath solution containing 140 mM Na^+ and 10 mM Ba^{2+}. (**C**) Compiled IV curves for peak Ba^{2+} (slow) currents measured in control or HERG expressing myotubes. The current density differed only at the two most positive voltages (40 and 50 mV), $^*p < 0.05$.

We find no effect of HERG on L-type current amplitude or Cav1.1 channel α subunit gene expression or protein abundance although HERG does increase myotube $[Ca^{2+}]i$ (over controls) in response to depolarization. Indeed, the fact that the HERG-modulated response is activated by depolarization and is nifedipine (10 μM) insensitive implicates ECCE, a Ca^{2+} release pathway that is insensitive to store depletion. *2-APB Block with Depolarization.* To further test if HERG is modulating ECCE, control and HERG-expressing myotubes were treated with vehicle or 2-APB, which will block ECCE (and SOCE)[32], and then depolarized to activate ECCE (and further inhibit SOCE) (Stiber et. al.[33] in Dirksen[19] and Kurebayashi and Ogawa[22]). Time resolved assays of $[Ca^{2+}]i$ using Fura-2 revealed that at 15 s in control cells, 2-APB inhibits (by 46.9%) the increase in $[Ca^{2+}]i$ that occurs in response to depolarization, but the change is not statistically significant ($p = 0.22$; Fig. 4A). However, the initial (up to 15 s) increase in $[Ca^{2+}]i$ that occurs in response to depolarization in HERG-over-expressing myotubes is inhibited 84.5% ($p < 0.005$; Fig. 4B) and the inhibition continues up to 57 s. Indeed, the 2-APB sensitive response during initial treatment (15 s) was significantly greater (75.3%; $p < 0.05$) in the HERG-expressing cells relative to controls (Fig. 4C). Thus, these data suggest that HERG overexpression in C_2C_{12} myotubes modulates ECCE.

The HERG channel modulates ryanodine receptor 1

Thapsigargin Block with Depolarization. Because RyR1 is a component of ECCE activity, we hypothesized that HERG could also be enhancing release of Ca^{2+} from intracellular stores. To test this, control and HERG-expressing myotubes were treated with either vehicle or Tg, which will deplete intracellular stores and activate SOCE, but have no effect on ECCE (Cherednichenko[17]; Lyfenko and Dirksen[20] in Dirksen[19]). The cells were then depolarized: (1) to release RyR1 from occlusion by Cav1.1 (i.e., DHPR) and enable Ca^{2+} release from the SR to the cytosol through the RyR1 channel[34], and (2) to inhibit SOCE (Stiber et. al[33] in Dirksen[19], Kurebayashi and Ogawa[22]). Indeed, depolarization activates the ECCE and pre-treatment with Tg will empty SR stores,thus, any inhibition noted in the Tg treated groups relative to vehicle treated groups will be predominantly a consequence of lowered SR stores. Time resolved $[Ca^{2+}]i$ assays using Fura-2 assays revealed thapsigargin did not significantly reduce the rise in $[Ca^{2+}]i$ upon KCl depolarization in control cells (Fig. 5A,B). However, the depolarization-induced rise in $[Ca^{2+}]i$ was significantly inhibited by thapsigargin in HERG-expressing myotubes relative to vehicle treated HERG-expressing myotubes for up to 40 s after depolarization (20 s, 49.4% inhibition, $p < 0.05$; 30 s, 72.7%, $p < 0.05$; 40 s, 77.1%, $p < 0.05$; Fig. 5C,D). Indeed, the Tg-sensitive portion of the response to depolarization was greater in HERG-expressing cells, with the difference in the Tg-sensitive response being statistically significant in earlier time points (~8–14 s; Fig. 5E). These data strongly suggest that a source of increased $[Ca^{2+}]i$ in the HERG-expressing myotubes is, at least in part, release of Ca^{2+} from SR stores. Thus, we decided to determine if HERG affects RyR1 activity. *Ryanodine Receptor Activation with Caffeine.* Membrane depolarization will uncouple RyR1 from occlusion by the DHPR and allow Ca^{2+} release from the SR to the cytosol through the RyR1 channel[34],therefore, we determined if HERG affects RyR1 activity specifically. Thus, RyR1 activity was assayed in control and HERG-expressing myotubes using caffeine to activate the RyR1 and the AUC of the change in 340/380 ratio was determined for each treatment group (Fig. 6). Caffeine treatment resulted in significant increases in $[Ca^{2+}]i$ in both the control and the HERG-over-expressing myotubes and this increase was significantly inhibited by ryanodine (90 μM) in both sets. A 2×3 ANOVA was used to compare

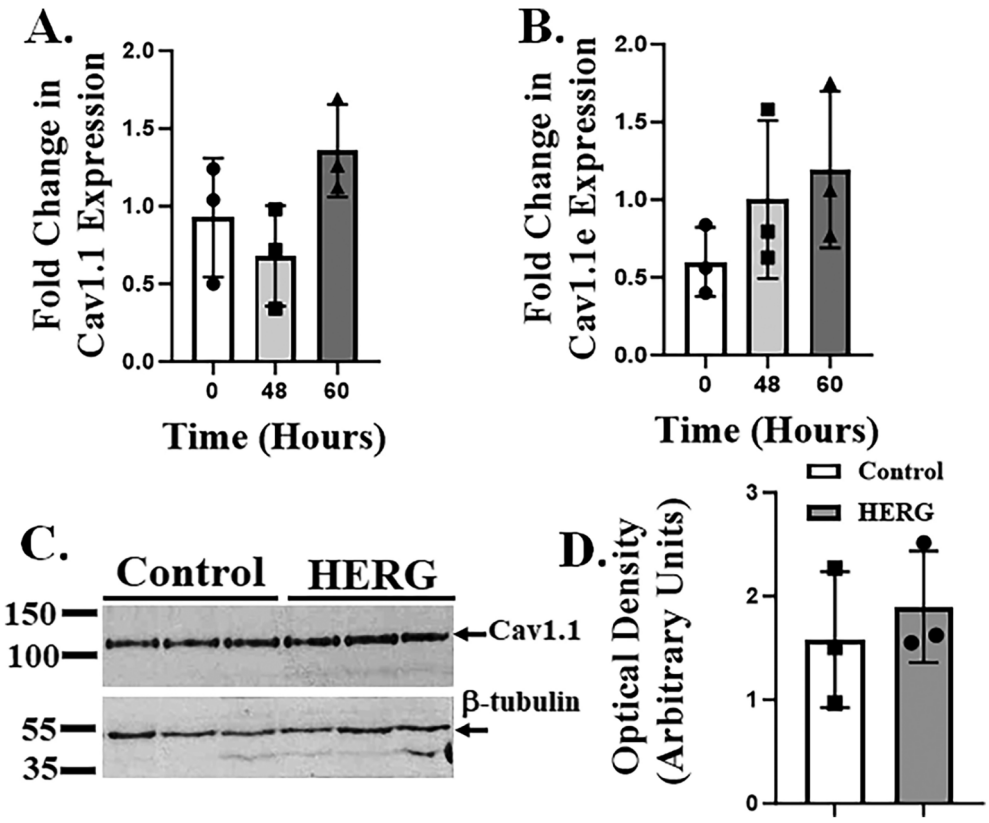

Fig. 3. Cav1.1 L-type Ca^{2+} channel gene expression and protein abundance are not affected by HERG expression in C_2C_{12} myotubes. (**A**,**B**) rtPCR assays reveal that mRNA levels of Cav1.1 (adult [**A**] and embryonic [Cav1.1e; **B**]) are not affected by HERG expression for up to 60 h post transduction. Expression of genes encoding either Cav1.2 or 1.3 was not detected in the myotubes. (**C**,**D**) Immunoblot (**C**) and optical density measures of protein bands (**D**) show that Cav1.1 protein abundance is not significantly affected at 48 h post HERG expression. (**A**,**B**,**D**) Bars represent mean fold changes in HERG-expressing cells over control cells, error bars represent standard deviations, and filled circles represent a single data point/replicate. A one-way ANOVA was used to analyze the data in panels (**A** and **B**). Data displayed in panel (**D**) were analyzed by a Student's t-test. (**A**,**B**) The data in panels (**A**) and (**B**) were derived from the same sample set. There were 9 replicates for each the control and the HERG-expressing cells, which were assayed at the three different time points (0, 46,and 60 h post-transduction). The data were calculated as HERG/control (see Methods) to produce ninefold change data points, three per time point. Thus, n = 9 data points total (i.e., ninefold changes—HERG-expressing over control cells). Two different sample sets were analyzed and yielded the same basic results; only one set is represented here. (**C**,**D**) The data shown in panels (**C**) and (**D**) were derived from a set of 6 cellular lysates (n = 6) composed of 3 control and 3 HERG-expressing myotube lysate samples. This experiment was performed with two different sample sets of which one is shown here. (See Additional file 2 for the second immunoblot and all full length Cav1.1 immunoblots.)

drug effects on $[Ca^{2+}]i$ in response to overexpression of HERG or lack thereof, control. The data show that, although the interaction between drug and HERG (or lack thereof) was not statistically significant ($p = 0.1373$), there was a statistically significant mean difference between HERG over-expressing and control cells across all drug treatments ($p = 0.0206$). The data demonstrate that HERG overexpression enhances caffeine-induced release of Ca^{2+} from the SR via RyR1 in C_2C_{12} myotubes.

The HERG channel affects $[Ca^{2+}]i$ by modulation of store operated calcium entry

The data support that ECCE contributes to the HERG-induced increase in $[Ca^{2+}]i$ in C_2C_{12} myotubes; however, HERG may also modulate other Ca^{2+} entry pathways. We assayed SOCE (see Methods) in control and HERG expressing cells under non-depolarizing conditions to eliminate any contribution from ECCE. Briefly, cells were loaded with Fura-2, pretreated with either vehicle or 2-APB (100 μM to block SOCE) for 30 min, and basal $[Ca^{2+}]_i$ levels were measured for 1 min. We then dispensed Tg (1 μM to deplete SR stores) into all wells. After 20 min, we dispensed Ca^{2+} (2.5 mM $CaCl_2$ final) into all wells to stimulate SOCE and monitored fluorescence for an additional 10 min. We normalized the data by subtracting the average of the 1 min baseline from all data points (Fig. 7A–C), which drove the control cell plus 2-APB treated replicates below baseline (Fig. 7A, C dark gray squares). In response to addition of extracellular $CaCl_2$, the $[Ca^{2+}]i$ increased greatly in the HERG over-expressing cells (Fig. 7A, B black triangles); however, the 340 nm/380 nm ratios acquired from the other cell

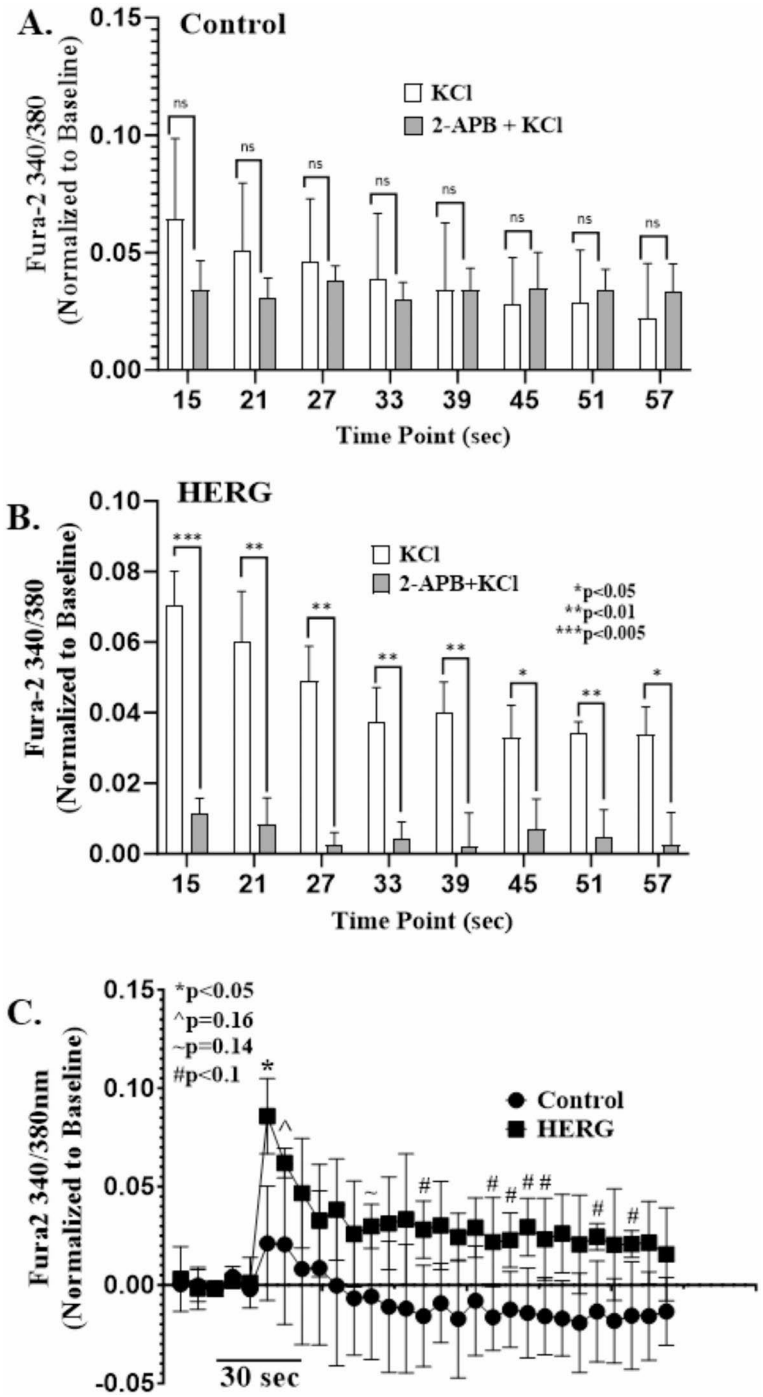

Fig. 4. Excitation coupled calcium entry (ECCE) is a source of the greater increase in intracellular calcium concentration ([Ca^{2+}]i) that is elicited in response to depolarization by KCl in HERG-expressing cells. (**A**) Initially, in control cells, 2-APB appears to have a mild, but statistically insignificant inhibitory effect on the initial mean increase in [Ca^{2+}]i that occurs in response to depolarization. (**B**) The 2-APB has a statistically significant inhibitory effect on the HERG-modulated increase in [Ca^{2+}]i that occurs in response to depolarization. (**C**) The initial 2-APB-sensitive currents differ significantly between the depolarized control and HERG-expressing myotubes, suggesting that a source of the initial HERG-modulated increase in [Ca^{2+}]i is extracellular. The [Ca^{2+}]i was evaluated by the ratiometric fluorescent Fura-2 dye and the 340/380 ratios were determined and normalized to baseline. The data of panels (**A**) and (**B**) were analyzed by a 2 × 2 ANOVA design for repeated measures; the interaction between HERG and treatment was not statistically significant. For panel (**C**), the mean difference and standard error of the mean difference were used to estimate *p* values using a comparison of means calculator (see Methods). The bars (**A**,**B**) and symbols (**C**) represent means of time frame units and error bars represent standard deviations. n = 24 (12 control and 12 HERG-expressing myotubes).

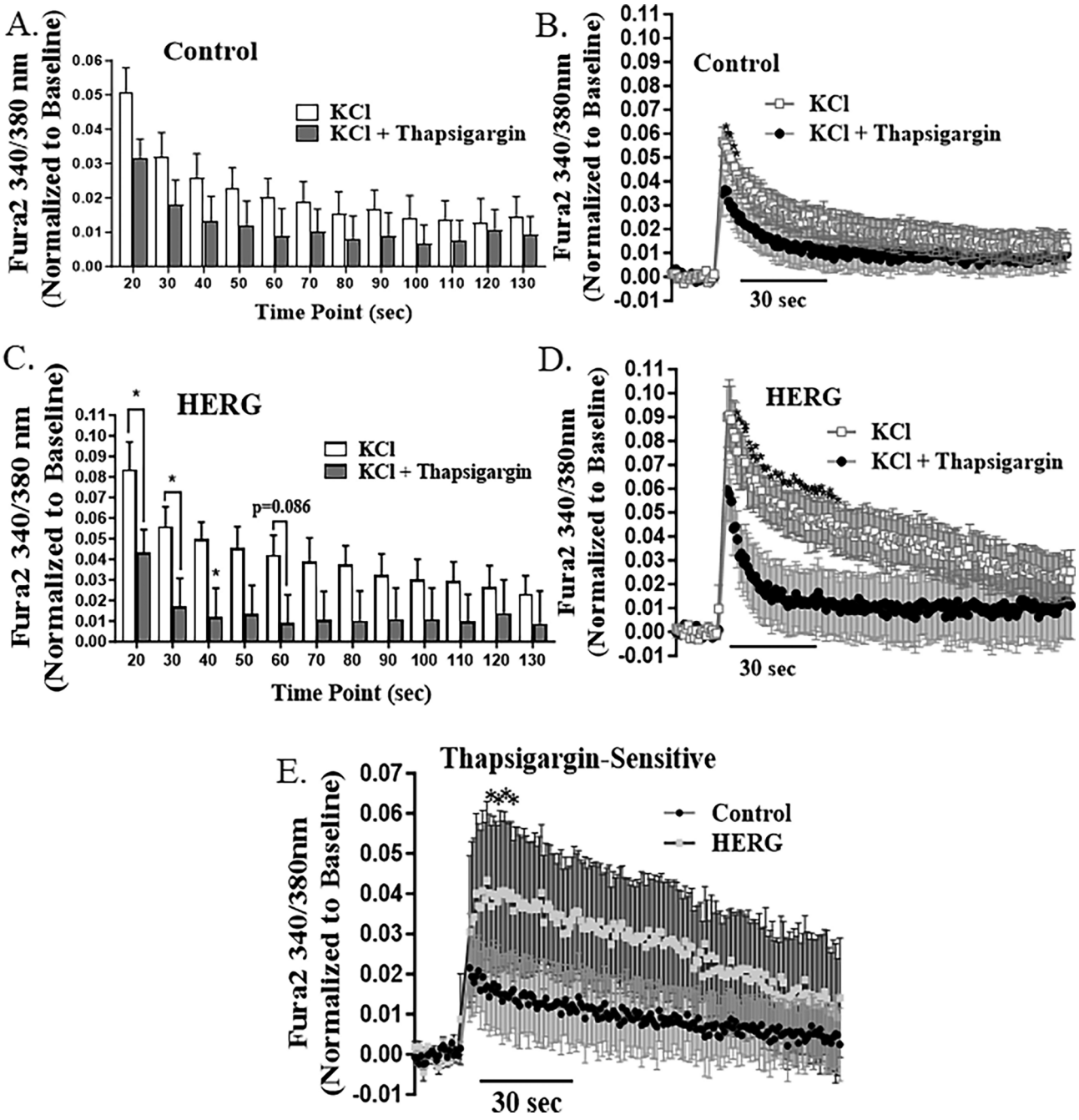

Fig. 5. Sarcoplasmic reticulum Ca^{2+} stores is a source of the greater increase in intracellular Ca^{2+} concentration ($[Ca^{2+}]i$) that occurs in response to depolarization by KCl (100 mM) in HERG-expressing cells. (**A**) In control cells, thapsigargin (Tg, 1 μM) has no statistically significant effect on $[Ca^{2+}]i$ in response to depolarization. (**B**) Change of $[Ca^{2+}]i$ in control cells in response to KCl treatment with and without Tg over time (cells from Figure **A**). (**C**) Thapsigargin has a significant inhibitory effect on the HERG-modulated increase in $[Ca^{2+}]i$ that occurs in response to depolarization. (**D**) Change of $[Ca^{2+}]i$ in HERG-expressing cells in response to KCl treatment with and without Tg over time (cells from Figure **C**). (**E**) Initial Tg-sensitive fluorescent ratios differ significantly between the depolarized control and HERG-expressing myotubes, suggesting that HERG may also affect release of Ca^{2+} from intracellular stores. The $[Ca^{2+}]i$ was evaluated by the ratiometric fluorescent Fura-2 dye and the 340/380 ratios were determined and normalized to baseline. The fluorescence ratios at noted timepoints (in panels **A** and **C**) were analyzed by a 2 × 2 ANOVA design for repeated measures. There was no significant interaction between HERG and treatment. For panel (**E**), the mean difference and standard error of the mean difference were used to estimate *p* values using a comparison of means calculator (see Methods). The bars (**A**,**C**) and symbols (**B**,**D**,**E**) represent mean fluorescence ratios (i.e., $[Ca^{2+}]i$ levels) and error bars represent standard deviation. n = 20 (10 control and 10 HERG-expressing myotubes). $^{*}p < 0.05$.

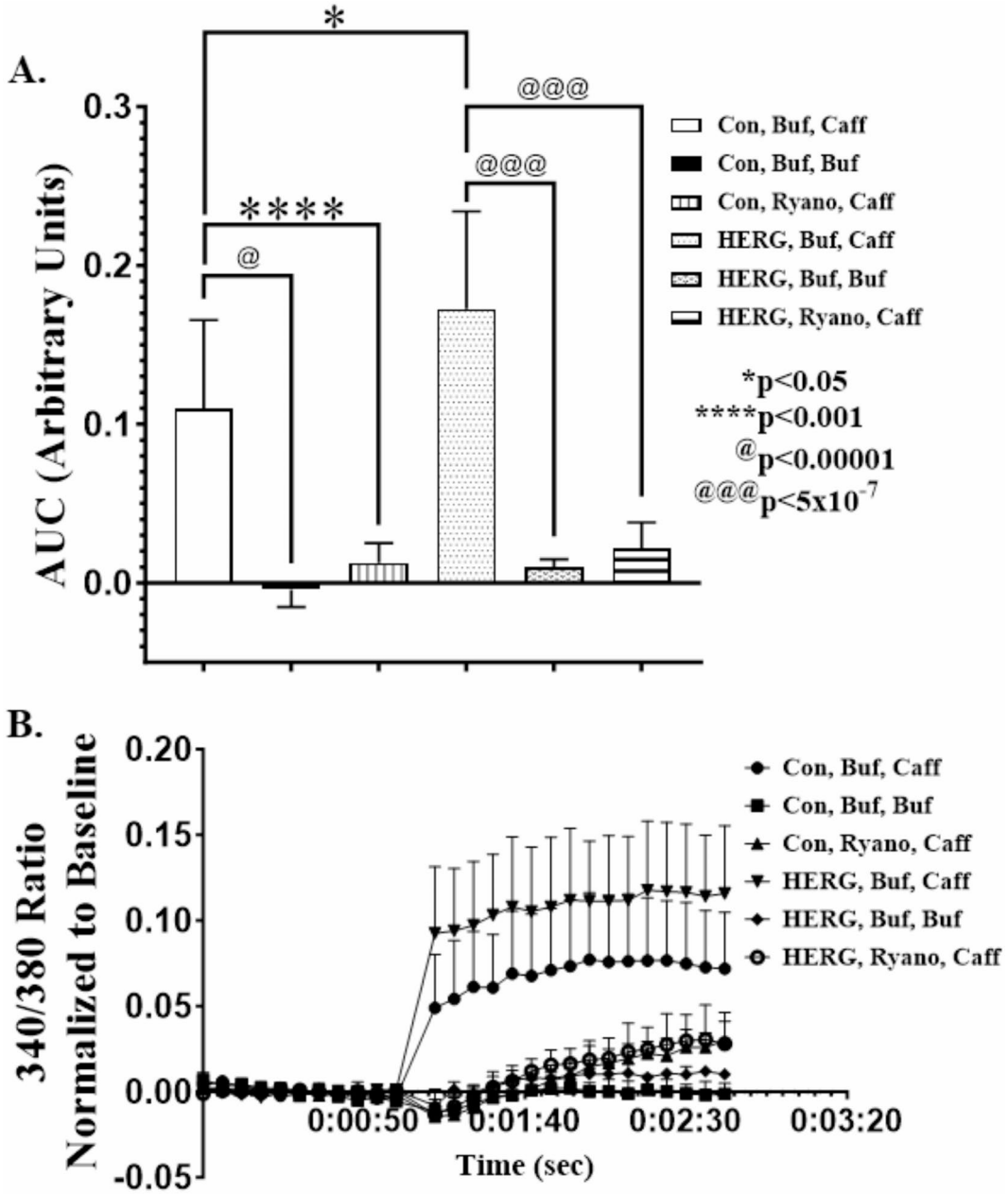

Fig. 6. HERG modulates ryanodine receptor-mediated Ca^{2+} release. (**A**) HERG-over-expressing myotubes exhibit a significantly greater increase in intracellular concentration ($[Ca^{2+}]i$) than control cells when treated with caffeine (10 mM); this response is significantly inhibited by ryanodine (90 uM) in both HERG-expressing and control myotubes, but the inhibition is more statistically significant in the HERG-over-expressing cells. n = 36 wells (18 wells of HERG-expressing myotubes and 18 wells of controls). (**B**) Representative line graph of a single assay of 24 wells. n = 24; the 24 wells consisted of 3 wells per each of six groups. The $[Ca^{2+}]i$ was evaluated by ratiometric fluorescent Fura-2 dye and the 340/380 ratios were determined and normalized to baseline. Areas under the curve (AUCs) were analyzed by one-way ANOVA and means were separated by Tukey's test. The bars (**A**) and symbols (**B**) represent means and error bars represent the standard deviation. Con = control cells transduced with the control adenovirus rather than the one encoding HERG. Buf = cells treated with the vehicle buffer rather than ryanodine. Ryano = ryanodine. Caff = caffeine.

groups decreased after calcium addition. The drop in $[Ca^{2+}]i$ upon sharply increasing extracellular Ca^{2+} was most apparent in the presence of 2-APB, and likely results from an off-target effect.

We compared the $[Ca^{2+}]i$ response to Tg before addition of extracellular Ca^{2+} in all treatment groups to determine if the rate of SR Ca^{2+} leak differs between control and HERG expressing cells (Fig. 7A–C). We determined the $[Ca^{2+}]_i$ AUCs for all treatment groups, from Tg injection until the addition of $CaCl_2$, and normalized (by subtraction) each time point to the average 1 min baseline. The normalized AUCs were compared using one-way ANOVA (Fig. 7D). There is no significant difference in the rise in $[Ca^{2+}]i$ that occurs in response

to Tg between control and HERG over-expressing cells; and the rise in $[Ca^{2+}]i$ is significantly inhibited by 2-APB in both groups. We then determined the percent rise in $[Ca^{2+}]i$ that is inhibited by 2-APB and compared the differences in inhibition between the expression groups (control and HERG) using a Student's t-test. We found that 2-APB inhibited 80.4 ± 11.3% of the Tg-induced $[Ca^{2+}]i$ increase in controls cells and 56.9 ± 8.1% in HERG expressing cells. This difference in 2-APB inhibition was significant ($p < 0.0005$), despite the fact that there is no difference in the total Ca^{2+} AUC stimulated by Tg between the two groups. This finding suggests that HERG induces Ca^{2+} leak from the ER that is sensitive to 2-APB. This source of leak isn't likely RYR1, because it is not blocked by 2-APB (Bilmen and Michelangeli 2002[69]). 2-APB does block IP_3 receptors in skeletal muscle[35], so it is possible that reduced levels of Casq1 also potentiate leak of SR Ca^{2+} through these channels, however, we have evidence that HERG does not affect IP3 signaling (Additional File 3).

To further assess the increase in SOCE in HERG expressing cells compared to controls, we normalized the data points acquired after calcium addition to the average of the 2 min baseline prior to calcium addition. We then calculated the AUCs for all data points and, using the absolute value of the total area under the curve, analyzed these data by one-way ANOVA (Fig. 7E). After this analysis, HERG over-expressing cells were found to produce a significantly greater increase in $[Ca^{2+}]i$ than all other groups, and this increase is significantly inhibited by 2-APB. Interestingly, although 2-APB-treated control cells demonstrate a smaller increase in $[Ca^{2+}]i$ than those treated with vehicle, this difference was not significant. This suggests there is no significant SOCE activity in the control cells. However, when we normalize (by subtraction) the data to the initial 1 min baseline, calculate these AUCs, and analyze the data by one-way ANOVA (Fig. 7F), we find that both the control and HERG over-expressing cells display significant SOCE activity. In this analysis, the increase in $[Ca^{2+}]i$ upon extracellular Ca^{2+} addition is significantly higher in HERG over-expressing cells than in controls. Again, we determined the percent rise in $[Ca^{2+}]i$ that is inhibited by 2-APB and compared the differences in inhibition between the expression groups (control and HERG) using a Student's t-test. 2-APB inhibited a greater percentage of the increase in $[Ca^{2+}]i$ in HERG expressing cells (76.7% ± 0.16%) than in controls (46.2 ± 0.37%; $p < 0.05$). Taken together, these data demonstrate that overexpression of HERG in C_2C_{12} myotubes elicits a greater SOCE response, although we do not know if the effect is direct or results from HERG-enhanced depletion of SR stores through enhanced RYR1 activity or both.

The HERG channel lowers abundance of calsequestrin1 mRNA and protein

Casq1 functions as both a Ca^{2+} buffer and a Ca^{2+} sensor in the SR and inhibits ryanodine receptor activity at cytosolic Ca^{2+} concentrations around 1 mM in skeletal muscle. It also inhibits the dimerization of the STIM1 protein necessary to activate the Orai1 channel for SOCE activity[26,29]. Because the Casq1 protein modulates RyR1 and STIM1, it has the potential to affect numerous pathways by which Ca^{2+} enters the cytosol, including ECC, ECCE, and SOCE. Therefore, we explored the effect of HERG-expression on Casq1 levels in C_2C_{12} myotubes. Total RNA was extracted from both control and HERG-expressing myotubes transduced at 200 MOI (n = 8, 4 control plates and 4 HERG plates) and HERG and Casq1 mRNA levels, relative to GAPDH, were compared using RT-qPCR. Myotubes transduced with adenovirus encoding HERG exhibited a 2.6-fold increase ($p < 0.02$) in HERG mRNA and a 0.83-fold decrease ($p < 0.05$) in Casq1 mRNA at 48 h after transduction (Fig. 8A). Further, both control and HERG-expressing myotubes were transduced at 200 MOI (n = 8, 4 control and 4 HERG) and lysates were immunoblotted using antibodies specific for either Casq1 or GAPDH (see Additional file 8). We measured the optical densities (OD) of the protein bands and noted a reduction in Casq1 protein (23.5%; $p = 0.081$) that approached, but did not reach significance (defined earlier as $p < 0.05$). To increase HERG expression levels, we transduced both control and HERG-expressing myotubes at 400 MOI (n = 8, 4 control and 4 HERG) and immunoblotted the lysates (Fig. 8 B-E) with antibodies specific for Casq1 and then (after stripping the PVDF membrane) with antibodies specific for GAPDH. We detected a full length Casq1 ~ 65 kD protein along with ~ 50 kD and ~ 40 kD Casq1 proteins which appear to be Casq1 degradation products (Fig. 8B). The mean OD of each Casq1 protein band was decreased in the HERG-expressing myotubes relative to control cells: the ~ 65 kD protein decreased 89.7% ($p = 0.012$); the ~ 50 kD protein decreased 66.3% ($p = 0.077$); and the ~ 40 kD protein decreased 80.8% ($p = 0.088$). When the OD values are combined per sample ("Total," Fig. 8E) and compared by a Student's t-test (HERG versus control), there is a 77% ($p = 0.036$) decrease in Casq1 protein abundance in HERG transduced myotubes. These data show that HERG overexpression produces a decrease in Casq1 protein abundance.

Discussion

Although ERG1A has been detected in the sarcolemma and t-tubules of heart muscle[4,36], the presence of ERG1A in skeletal muscle was not reported until we detected it in the sarcolemma of atrophying skeletal muscle[5,7]. We reported that overexpression of ERG1A in mouse *Gastrocnemius* muscle enhances proteolysis through up-regulation of UPP activity by increasing the protein (and mRNA) abundance(s) of the muscle specific UPP E3 ligase MuRF1[5,8,9]. Further, we showed that HERG overexpression in C_2C_{12} myotubes also produces an increase in MuRF1 protein abundance and, interestingly, in both basal $[Ca^{2+}]i$ and calpain activity[10]. Because elevated $[Ca^{2+}]i$ is known to play a role in atrophy[37], we sought to determine by what mechanism(s) HERG regulates $[Ca^{2+}]i$.

ERG1A is a sarcolemmal membrane-bound voltage-gated K^+ channel, thus it is feasible that it might in some way affect the L-type voltage-gated Ca^{2+} channel(s) also located in the sarcolemma. We reasoned that the ERG1A channel would not likely hyperpolarize the skeletal myocyte membrane appreciably because it's role in cardiac tissue is to facilitate repolarization of the action potential and prevent early after depolarizations[38]. We hypothesized, however, that the channel's presence in the skeletal muscle sarcolemma might in some way modulate the current amplitude or abundance of the Cav1.1 Ca^{2+} channels (DHPRs) also located there. Indeed, the depolarization-induced calcium flux in the HERG over-expressing cells was greater than in control cells;

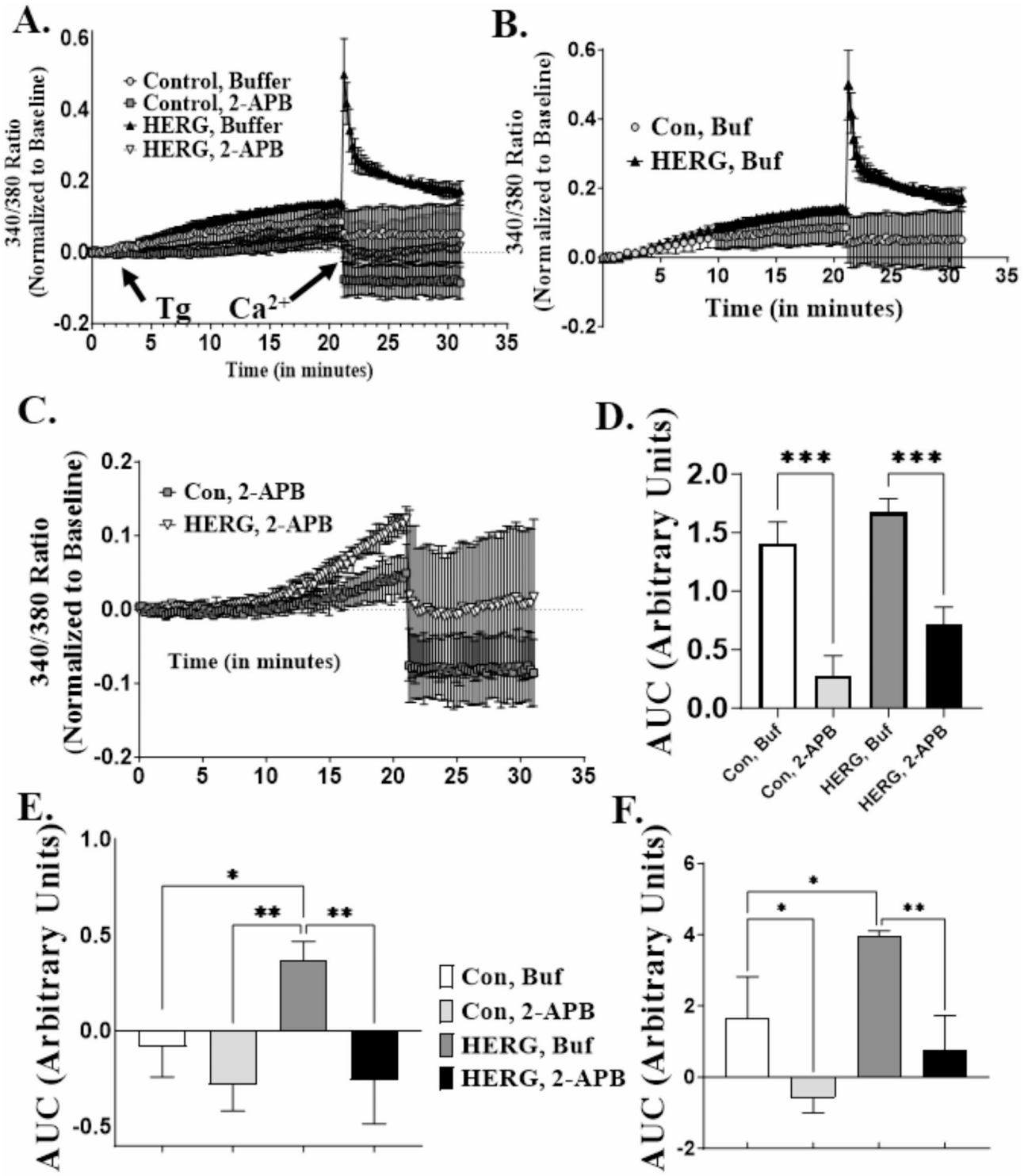

however, the difference between the KCl-stimulated Ca^{2+} increase in control and the HERG over-expressing cells is not significantly inhibited by nifedipine (10 μM) and thus cannot be accounted for by L-type channel mediated Ca^{2+} influx. Thus, we postulated that it could result from activation of the ECCE. Indeed, the ECCE is an extracellular Ca^{2+} entry pathway that is activated by prolonged and repetitive depolarization (e.g., 100 mM KCl), but is not sensitive to block by 10 μM nifedipine[15]. Block of ECCE activity in primary mouse muscle cultures requires a higher concentration of nifedipine (50 μM[15]). Thus, to test for possible HERG modulation of ECCE, we applied 2-APB (known to block ECCE activity;[17]), and discovered that the HERG-modulated, depolarization-induced increase in $[Ca^{2+}]i$ is inhibited by 2-APB. SOCE, which allows calcium entry from the extracellular milieu, is also blocked here by both depolarization and 2-APB[17]. Further, the assay conditions should not significantly deplete the SR, so we do not expect relevant activation of SOCE[22,33]. Therefore, here we have evidence that HERG modulates $[Ca^{2+}]i$ (at least in part) through modulation of ECCE.

◀**Fig. 7**. HERG modulates SOCE. (**A**) SOCE Activity in control and HERG over-expressing myotubes. Graphic shows changes in 340/380 nm ratios over time as measured by fluorescence (Fura-2 dye) in response to thapsigargin (Tg, 1 μM, 20 min) and then $CaCl_2$ (2.5 mM, 10 min) treatments with and without 2-APB (100 μM). Ratios represent intracellular calcium concentration ($[Ca^{2+}]i$). All time points were normalized (by subtraction) to the average 1 min initial baseline (except panel **E**). (**B**) SOCE activity in Control and HERG over-expressing myotubes in the absence of 2-APB. HERG over-expressing cells exhibit a significantly greater increase in $[Ca^{2+}]i$ than control cells when treated with high calcium after depletion of SR calcium stores. (**C**) SOCE activity in control and HERG overexpressing myotubes treated with 2-APB. 2-APB blocks the rise in $[Ca^{2+}]i$ that would occur upon addition of extracellular Ca^{2+}. (**D**) $[Ca^{2+}]i$ response to Tg. Graphic showing the areas under the curve (AUCs) resulting from Tg treatment (panel **A** data). For each treatment group, the 340/380 nm ratios were determined at each timepoint after Tg addition and before calcium treatment. The timepoint ratios were normalized and the AUCs were determined. (**E**) HERG enhances SOCE activity. For each treatment group, the 340/380 nm ratios were determined at each timepoint after calcium addition and normalized (by subtraction) to the average "baseline" measured for two minutes prior to calcium addition to correct for differences in $[Ca^{2+}]i$ occurring during incubation with Tg. (**F**) SOCE activity normalized to initial one min baseline. Here, for each treatment group, the 340/380 nm ratios were determined at each timepoint after calcium addition and normalized to the initial baseline. Statistics. The AUCs for time points after treatments were calculated per treatment group and analyzed by one-way ANOVA using GraphPad Prism. When different, means were separated by Tukey's test. The symbols (**A**–**C**) and bars (**D**–**F**) represent means and error bars represent the standard deviation. n = 12 wells per viral treatment (6 wells of HERG-expressing myotubes and 6 wells of controls; per viral treatment, 3 wells received 2-APB and 3 received vehicle). For panels (**D**) and (**F**), the change in AUCs resulting from 2-APB within cell expression group (control or HERG) were calculated by subtracting all 2-APB treated replicates from all non-treated replicates within a cell expression group and then compared between expression group (control versus HERG) using a Student's t-test.

The ECCE activity unit is believed to be composed of Cav1.1, RyR1, and possibly an (as yet) unrevealed calcium conducting and/or modulating moiety[11,19] (Bannister and Beam 2013[68]; Friedrich et. al. 2010) Because of the involvement of RyR1 in ECCE activity, we hypothesized that HERG might also affect release of calcium from intracellular stores through RyR1. To test this, we investigated the effect of SR depletion (induced by Tg inhibition of SR Ca^{2+}-ATPase) on the HERG-modulated elevation of $[Ca^{2+}]i$. Indeed, we discovered that (at least a portion of) the HERG-modulated, depolarization-induced increase in $[Ca^{2+}]i$ is sensitive to store depletion by Tg, suggesting that HERG may also activate release of Ca^{2+} from intracellular stores[17,18]. To explore this further, we investigated the effect of HERG on RyR1 activity more directly. RyR1 is a caffeine activated, voltage-gated protein[39] which will allow calcium release from the SR[34]. Here we demonstrate that HERG overexpression enhances the increase in $[Ca^{2+}]i$ that occurs with caffeine treatment in myotubes; and this effect is blocked by inhibitory concentrations of ryanodine, suggesting that HERG modulates RyR1 activity. Further, we note that, although the increase in $[Ca^{2+}]i$ that occurs with SERCA inhibition (by Tg) is not affected by HERG, the percent inhibition of the rise in $[Ca^{2+}]i$ resulting from 2-APB treatment (SOCE block) of these Tg-treated cells is significantly lower in HERG over-expressing cells than in control. Thus, the $[Ca^{2+}]i$ enhancement likely represents calcium leak through RYR1 (Fig. 6), which indeed is not inhibited by 2-APB (Bilmen and Michelangeli 2002[69]). Additionally, IP3 signaling could also be responsible for the HERG enhanced increase in $[Ca^{2+}]i$ during Tg treatment. IP3 signaling is inhibited by 2-APB (Bilmen and Michelangeli 2002[69]); however, the ATP-stimulated increase in $[Ca^{2+}]i$ that occurs upon PLC activation (and presumably activation of IP_3 receptors) was not different between control and HERG over-expressing myotubes (Additional File 3). Thus, it is not likely that this calcium "leak" is a consequence of IP3 signaling. It is also possible that HERG could be affecting TRP channels to increase $[Ca^{2+}]i$; these channels are also blocked by 2-APB. This needs more detailed exploration. Our data also suggest that HERG modulates SOCE; however, it is not clear whether this HERG-induced increase in SOCE activity is a consequence of stores depletion subsequent to RyR1 activation OR of direct modulation of SOCE pathway components. This remains to be explored.

Our data confirm that HERG overexpression affects $[Ca^{2+}]i$ in cultured myotubes. Further, it strongly suggests that it does so (at least in part) by enhancing RyR1 activity, a known component of the ECCE. Indeed, we also show that ECCE activity is enhanced by HERG overexpression. However, our data also show that HERG does not affect myotube L-type current amplitude over time nor does it modulate Cav1.1 protein abundance nor mRNA levels. These findings could suggest that an L-type channel (specifically Cav1.1) is not part of ECCE activity OR that, if it is, then pore permeation of this channel by calcium is not necessary for ECCE activity (as is suggested by earlier work;[17]). Nonetheless, it has been shown that the characteristics of ECCE calcium flux are those of L-type currents and that presence of Cav1.1 L-type channels are necessary for ECCE[15,17]. Interestingly, however, one report investigating calcium flux in mouse skeletal muscle fibers describes a voltage-activated Mn^{2+} pathway which is "parallel to," but distinct from, the L-type voltage-activated calcium channel and has properties which suggest it could contribute to ECCE activity[40]. Perhaps this "parallel" entity may be a more likely candidate for current conduction in the ECCE.

Because our data suggest that ERG1A modulates both RyR1 and ECCE activities, as well as SOCE activity, we conjectured that ERG1A could be affecting an entity that modulates all three Ca^{2+} entry pathways. We hypothesized that Casq1, a Ca^{2+} sensing and buffering protein detected prominently within the SR milieu, would be a likely candidate. Casq1 binds and releases calcium within the SR in a manner which maintains appropriate physiological calcium concentrations there. If abundance of this protein were to decrease, then there would be a higher level of free calcium in the SR available for release in response to any signal for SR calcium efflux. A greater

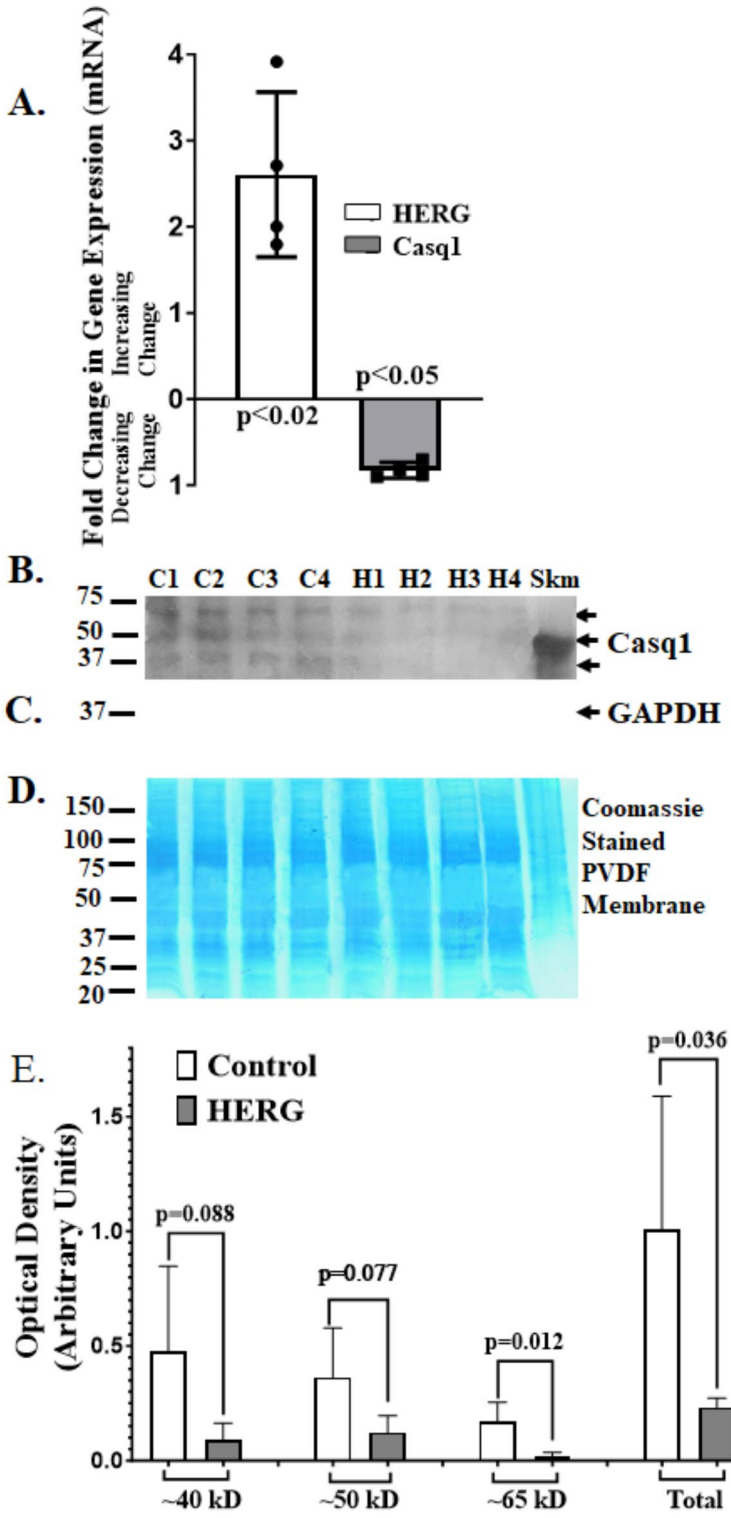

release in free calcium from the SR would result in a higher $[Ca^{2+}]i$. Indeed, our immunoblot data demonstrate that Casq1 protein abundance is significantly lower in HERG-expressing cells than in controls. Interestingly, one known mechanism by which Casq1 modulates $[Ca^{2+}]i$ is by interacting with RyR1. At ≥ 5 mM Ca^{2+} concentration in the SR ($[Ca^{2+}]_{SR}$), Casq1 is polymerized and binds/stores high Ca^{2+} levels near the junctional SR membrane to allow quick release of Ca^{2+} during excitation contraction coupling; this action also buffers Ca^{2+} and regulates SR osmolarity (Perni et. al.[41]; reviewed in Woo et. al.[42] and in Wang and Michalak[43]). At ~ 1 mM $[Ca^{2+}]_{SR}$, although still polymerized and binding Ca^{2+} ions, Casq1 binds and inhibits RyR1 so that Ca^{2+} cannot pass through this channel into the cytosol[44,45]. At $[Ca^{2+}]_{SR} \leq 100$ µM, Casq1 depolymerizes, thus lowering its Ca^{2+} binding capacity and releasing free Ca^{2+} within the SR as it also dissociates from RyR1. The interaction between RyR1 and Casq1 requires other SR junctional proteins such as junctin and triadin[43]. Indeed, removing Casq1 from the RyR1-junctin-triadin complex creates an increased probability and duration of RyR1 channel opening,adding the

◀**Fig. 8**. Calsequestrin 1 (Casq1) mRNA and protein levels are reduced in C_2C_{12} myotubes at 48 h after transduction with 400 MOI HERG encoded virus relative to myotubes transduced with control virus. (**A**) Fold changes in HERG and Casq1 mRNA levels in response to transduction with HERG-encoded adenovirus. HERG mRNA increased 2.6-fold ($p < 0.02$) in HERG-transduced myotubes and Casq1 mRNA decreased 0.83-fold ($p < 0.05$) in the HERG-expressing cells. (**B**) Control and HERG-expressing myotube lysates immunoblotted with antibody specific for Casq1 protein. (**C**) Control and HERG-expressing myotube lysates immunoblotted with antibody specific for the "house-keeping" protein GAPDH. (**D**) PVDF membrane stained with Coomassie blue to confirm equal sample loading in lanes. (**E**) Normalized optical densities (OD) of individual Casq1 proteins and of Casq1 proteins combined ("Total") from immunoblot. Mean ODs of control and HERG-expressing cells (within each protein) were analyzed by Student's T-test. Bars represent average OD and error bars denote the standard deviation. n = 8, 4 control groups and 4 HERG-expressing groups. Skm = mouse skeletal muscle. All full blots are available in Additional file 3.

Casq1 back to this RyR1 complex yields decreased channel opening duration[44,46]. Thus, Casq1 essentially blocks RyR1 activity at resting Ca^{2+} concentrations. Further, RyR1 is a component of ECCE and, although it is not believed to be the Ca^{2+}-passing entity in this extracellular Ca^{2+} entry pathway (reviewed in Dirksen[19] and Cho et al.[11]), ECCE activity is modulated by ryanodine treatment: accentuated by low dose and blocked by high doses as is the RyR1 protein[17,47,48]. Thus, it is possible that our observed effect of ERG1A on ECCE is through the lowered Casq1 abundance and consequent decreased RyR1 activity. Although less likely, it could also be through Casq1 modulation of Cav1.1. Indeed, a complex of Casq1 and the transmembrane protein JP45 modulate Cav1.1[49] and ablation of both JP45 and Casq1 proteins enhances ECCE activity in mouse skeletal muscle[50]. However, as we demonstrate here, ERG1A modulation of Cav1.1 current conduction is not likely to occur. However, ERG1A could also be affecting $[Ca^{2+}]i$ through direct Casq1 modulation of SOCE. Casq1 regulates SOCE by inhibiting STIM1 aggregation, thus decreasing the entry of Ca^{2+} through this extracellular pathway[27,29]. Thus, lowered Casq1 abundance could result in less inhibition of STIM1 aggregation and increased $[Ca^{2+}]i$.

Indeed, down-regulation of Casq1 protein abundance could increase $[Ca^{2+}]i$ through interaction of multiple mechanisms and play a role in the skeletal muscle atrophy induced by ERG1A. Work with Casq1 knockout mice supports this idea. Casq1 knockout mice were viable, but skeletal muscle from these mice exhibited enhanced sensitivity to caffeine, an increased magnitude of Ca^{2+} release in response to depolarization, and an increase in resting $[Ca^{2+}]i$, likely because Casq1 modulates RyR1 activity[51]. Thus, these data support the idea that a decrease in Casq1 would result in an increase in both resting $[Ca^{2+}]i$ and Ca^{2+} release in response to depolarization (and other SR calcium release stimuli). Further, Casq1 ablation results in formation of SR-stacks which contribute to formation of Ca^{2+} entry units (CEUs), which are intracellular junctions that modulate SOCE[51,52]. These SR-t-tubule junctions within the I-band of Casq1 null mice muscle represent pre-assembled CEUs that provide a mechanism for constitutively active SOCE, hypothesized to be a calcium source compensating for the lower Ca^{2+} concentration within the SR[53–55]. Constitutively active SOCE, whether induced by direct HERG action on pathway components or through HERG-induced lowered SR calcium stores (resulting from enhanced RyR1 activity) could explain the increased basal intracellular Ca^{2+} detected in C_2C_{12} myotubes over-expressing HERG[10]. Interestingly, Casq1-ablated mice also presented with a reduction in body weight compared to wild type (WT)[56] (Paolini et al. 2015[70]) and with skeletal muscle atrophy, which manifested as a significant decrease in both EDL muscle fiber cross sectional area and grip strength (Paolini et al. 2015[70]). The atrophy likely also results from the increase in expression of certain atrogenes (i.e., CathepsinL, Psmd1, Bnip3, and Atrogin) also reported by this group. Additionally, it could be (at least in part) a result of an increase in Ca^{2+} dependent calpain activity induced by the increase in $[Ca^{2+}]i$ These results are consistent with the finding that HERG overexpression in *Gastrocnemius* muscle and in C_2C_{12} myotubes induces skeletal muscle atrophy[5,10].

An important question left unanswered by this study is: How does ERG1A overexpression result in lowered Casq1 protein levels (Fig. 9A)? Interestingly, our RTPCR data reveal that ERG1A overexpression decreases Casq1 gene expression. Indeed, lowered levels of Casq1 mRNA are likely to result in a lower abundance of the encoded protein (as observed here); however, how the large membrane bound HERG protein affects transcription of Casq1 will require study. We hypothesize this modulation likely occurs by HERG interaction with small signaling (perchance DNA-binding) proteins that interact with regions of the HERG N-terminus, specifically the PAS-PAC sequence. HERG may also affect Casq1 mRNA levels through post-transcriptional modulation. Additionally, we have shown that ERG1A up-regulates UPP activity by increasing the abundance of the MuRF1 E3 ligase in mouse skeletal muscle and in C_2C_{12} myotubes[5,10]. Therefore, we hypothesize that ERG1A could also enhance the degradation of the Casq1 protein by increasing UPP activity; indeed, there are ubiquitinylation sites on Casq1 (https://www.phosphosite.org/homeAction). These areas remain to be explored.

Perhaps the most fundamental question regarding the role of ERG1A in skeletal muscle atrophy is: "What induces increased levels of the ERG1A channel in skeletal muscle (Fig. 9B)?" ERG1A is up-regulated in skeletal muscle undergoing atrophy as a consequence of unloading, cancer cachexia and denervation[5,7] (Pond et al. 2014[71], Hockerman et al. 2014[8]). It is likely, therefore, that some factor common to these conditions induces expression of ERG1A. Perhaps simply a decrease in stimulation of the muscle contributes in some way. This is another area that remains to be explored.

An important limitation of this study is that all of the work presented here has been performed in cultured myotubes rather than in animals or primary isolated skeletal muscle fibers or tissue explants, which would provide a more holistic view. Indeed, muscle contraction, force generation, metabolic function, etc. are highly affected by/dependent upon specific tissue structural characteristics and the interaction of various cells. The cultured myotubes do not have complete contractile apparati and lack access to extracellular matrix materials

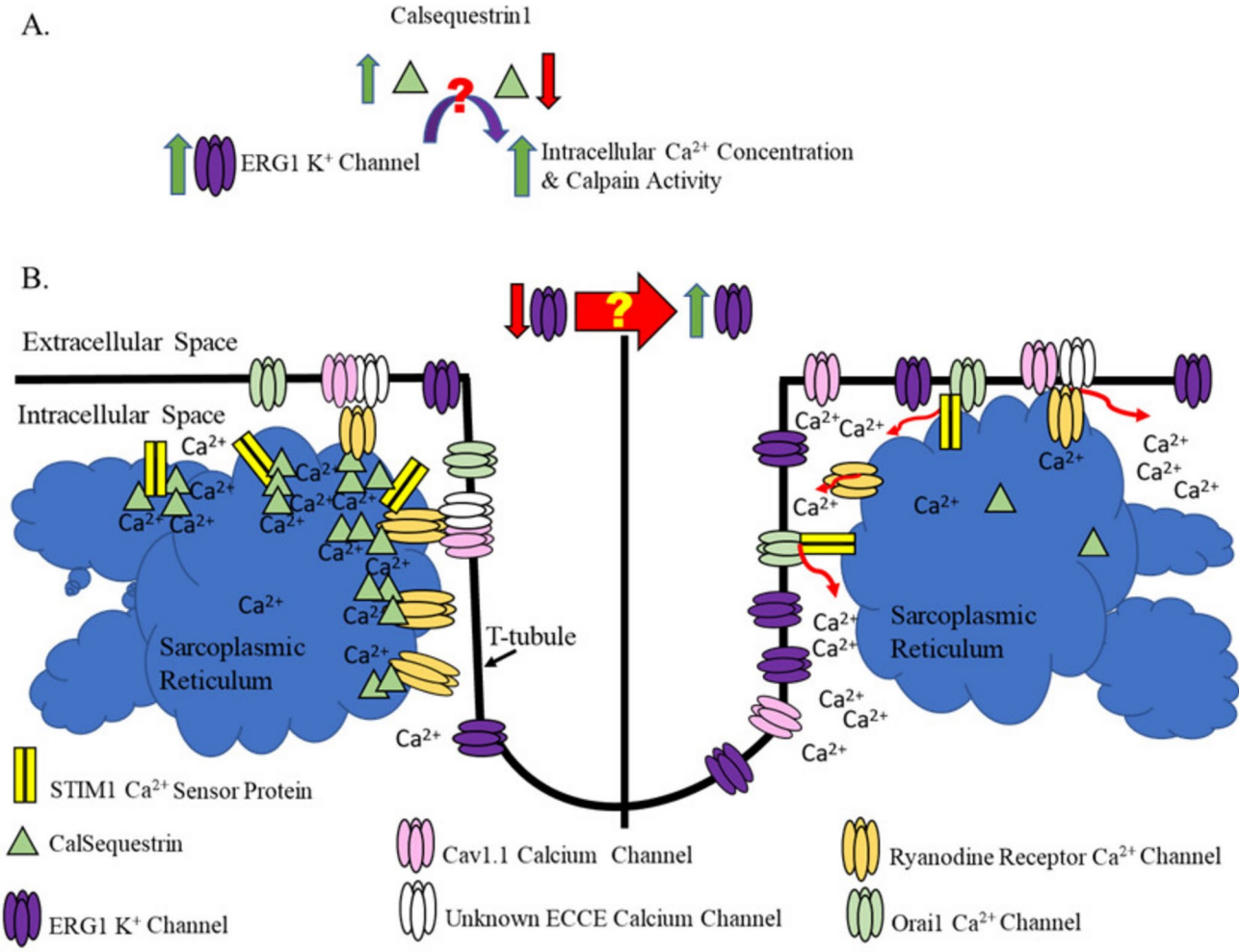

Fig. 9. HERG increases intracellular Ca^{2+} concentration by decreasing abundance of the Ca^{2+} binding/buffering protein Calsequestrin1. Two important questions are: (**A**) How does ERG1A decrease Calsequestrin1?; and (**B**) What induces increased levels of the ERG1A channel itself?

and ultrastructure which help localize growth factors and glycoproteins necessary for growth and tissue metabolism (reviewed in Smith and Meyer[57] and Gillies and Lieber[58]). However, the isolated, cultured cells allow for study of skeletal muscle cell physiology without interference from other tissue type effects and, thus, yield a more accurate model for study of $[Ca^{2+}]i$ in skeletal muscle cells specifically. Other limitations with this work include the use of an adenoviral vector to overexpress the HERG gene. Although we do control for general viral perturbations by comparing our HERG over-expressing myotubes to control myotubes transduced with the same vector not encoding HERG, we still are using an "overexpression" model. That is, the abundance of HERG protein produced in response to transduction, as well as the cellular response to the HERG protein, may or may not be realistic in terms of how muscle cells respond in vivo to certain atrophic stimuli and the subsequent upregulation of HERG. However, we have shown that transduction of C_2C_{12} myotubes with HERG results in decreased myotube area and increased MuRF1 E3 ligase protein abundance as occurs when ERG1A is electro-transferred into mouse skeletal muscle[5,9,10]. As well, we have shown that overexpression of HERG in C_2C_{12} myotubes yields an increase in both $[Ca^{2+}]i$ and subsequent calpain activity[10]. Indeed, decreased myofiber size and increased UPP E3 ligase protein abundances as well as increased $[Ca^{2+}]i$ and calpain activity are known characteristics of atrophic skeletal muscle[37]. Thus, despite these potential limitations, this study has relevance to muscle health and muscle pathologies because perturbances (e.g., increases) in $[Ca^{2+}]i$ can have detrimental and even severe effects on muscle tissue[37,59,60].

Conclusions

This study provides a potential mechanism to explain how upregulation of ERG1A might contribute to increased $[Ca^{2+}]i$ and, thus, atrophy in skeletal muscle. Here, we describe downregulation of Casq1 protein (and mRNA) abundance in response to HERG overexpression. We also report amplification of Ca^{2+} release from the SR via RyR1 in addition to increased ECCE and SOCE activities in myotubes over-expressing HERG. It is likely that HERG enhancement of RyR1 activity, through decreased Casq1 abundance, is increasing $[Ca^{2+}]i$. We suggest that the HERG-modulated effect on the ECCE occurs through modulation of RyR1. We further postulate that HERG

overexpression may constitutively enhance SOCE activity perhaps by lowering the concentration/availability of free calcium in the SR and/or by the decreased inhibition of STIM1 resulting from lowered Casq1. A greater understanding of the mechanism(s) by which this K^+ channel affects $[Ca^{2+}]i$ could identify suitable targets for development of therapies for atrophy and numerous other skeletal muscle pathologies. Indeed, because ERG1A is a component of the I_{Kr} channel responsible for repolarization of the cardiac action potential, it is not a tractable pharmacological target for treatment of atrophy. Finally, because ERG1A channels are also found in other tissues (e.g., brain, intestinal smooth muscle cells, tumor cells, heart, etc.)[61,62] (Babcock and Li 2013)[67], research of this mechanism may ultimately invite a broader interest, addressing ERG1A-modulated Ca^{2+} dysregulation in other tissues[63–66].

Data availability

The datasets used and/or analyzed during the current study are available from the corresponding author on reasonable request.

Received: 19 November 2024; Accepted: 10 March 2025
Published online: 19 March 2025

References

1. London, B. et al. Two isoforms of the mouse *Ether-a-go-go*-related gene coassemble to form channels with properties similar to the rapidly activating component of the cardiac delayed rectifier K^+ current. *Circ. Res.* **81**, 870–878 (1997).
2. Lees-Miller, J. P., Kondo, C., Wang, L. & Duff, H. J. Electrophysiological characterization of an alternatively processed ERG K^+ channel in mouse and human hearts. *Circ. Res.* **81**(5), 719–726 (1997).
3. Curran, M. E. et al. A molecular basis for cardiac arrhythmia: Herg mutations cause long QT syndrome. *Cell* **80**, 795–803 (1995).
4. Jones, E. M. C., Roti Roti, E. C., Wang, J., Delfosse, S. A. & Robertson, G. A. Cardiac IKr channels minimally comprise hERG1a and 1b subunits. *J. Biol. Chem.* **279**, 44690–44694 (2004).
5. Wang, X. et al. Merg1a K^+ channel induces skeletal muscle atrophy by activating the ubiquitin proteasome pathway. *FASEB J.* **20**(9), 1531–1533 (2006).
6. Zampieri, S. et al. The ERG1A K^+ channel is more abundant in *Rectus abdominis* muscle from cancer patients than in that from healthy humans. *Diagnostics* **11**(10), 1879. https://doi.org/10.3390/diagnostics11101879 (2021).
7. Anderson, L. B. et al. MERG1A protein abundance increases in the atrophied skeletal muscle of denervated mice, but does not affect NFκB activity. *J. Neuropathol. Exp. Neurol.* **80**(8), 776–788. https://doi.org/10.1093/jnen/nlab062 (2021).
8. Hockerman, G. H. et al. The Ubr2 gene is expressed in skeletal muscle atrophying as a result of hind limb suspension, but not Merg1a expression alone. *Eur. J. Transl. Myol.* **24**(2), 207–214 (2014).
9. Pond, A. L. et al. The MERG1a channel modulates skeletal muscle *MuRF1*, but not *MAFbx*, expression. *Muscle Nerve* **49**(3), 378–388 (2013).
10. Whitmore, C. et al. The ERG1a potassium channel increases basal intracellular calcium concentration and calpain activity in skeletal muscle cells. *Skeletal Muscle* **10**, 1–15. https://doi.org/10.1186/s13395-019-0220-3 (2020).
11. Cho, C. H., Woo, J. S., Perez, C. F. & Lee, E. H. A focus on extracellular Ca^{2+} entry into skeletal muscle. *Exp. Mol. Med.* **49**, e378. https://doi.org/10.1038/emm.2017.208 (2017).
12. Bal, N. C. et al. Sarcolipin is a newly identified regulator of muscle-based thermogenesis in mammals. *Nat. Med.* **18**, 1575–1579. https://doi.org/10.1038/nm.2897 (2012).
13. Bruton, J. D. et al. Increased fatigue resistance linked to Ca^{2+}-stimulated mitochondrial biogenesis in muscle fibers of cold-acclimated mice. *J Physiol (Lond)* **588**, 4275–4288 (2010).
14. Tu, M. K., Levin, J. B., Hamilton, A. M. & Borodinsky, L. N. Calcium signaling in skeletal muscle development, maintenance and regeneration. *Cell Calcium* **59**, 91–97 (2016).
15. Bannister, R. A., Pessah, I. N. & Beam, K. G. The skeletal L-type Ca^{2+} current is a major contributor to excitation-coupled Ca^{2+} entry. *J. Gen. Physiol.* **133**(1), 79–91 (2009).
16. Yang, T., Allen, P. D., Pessah, I. N. & Lopez, J. R. Enhanced excitation-coupled calcium entry in myotubes is associated with expression of RyR1 malignant hyperthermia mutations. *J. Biol. Chem.* **282**, 3747–37478 (2007).
17. Cherednichenko, G. et al. Conformational activation of calcium entry by depolarization of skeletal myotubes. *PNAS* **101**, 15793–15798 (2004).
18. Hurne, A. M. et al. Ryanodine receptor type 1 (RyR1) mutations C4958S and C4961S reveal excitation-coupled calcium entry (ECCE) is independent of sarcoplasmic reticulum store depletion. *J. Biol. Chem.* **280**, 36994–37004 (2005).
19. Dirksen, R. T. Checking your SOCCs and feet: The molecular mechanisms of Ca^{2+} entry in skeletal muscle. *J. Physiol.* **13**, 3139–3147 (2009).
20. Lyfenko, A. D. & Dirksen, R. T. Differential dependence of store-operated and excitation-coupled calcium entry in skeletal muscle on STIM1 and Orai1. *J. Physiol.* **586**, 4815–4824 (2008).
21. Lee, E. H., Cherednichenko, G., Pessah, I. N. & Allen, P. D. Functional coupling between TRPC3 and RyR1 regulates the expressions of key triadic proteins. *J. Biol. Chem.* **281**, 10042–10048 (2006).
22. Kurebayashi, N. & Ogawa, Y. Depletion of Ca^{2+} in the sarcoplasmic reticulum stimulates Ca^{2+} entry into mouse skeletal muscle fibres. *J. Physiol.* **533**, 185–199 (2001).
23. Feske, S. et al. A mutation in Orai1 causes immune deficiency by abrogating CRAC channel function. *Nature* **441**, 179–185 (2006).
24. Roos, J. et al. STIM1, an essential and conserved component of store-operated Ca^{2+} channel function. *J. Cell Biol.* **169**, 435–445 (2005).
25. Vig, M. et al. CRACM1 is a plasma membrane protein essential for store-operated calcium entry. *Science* **312**, 1220–1223 (2006).
26. Jeong, S. Y., Oh, M. R., Choi, J. H., Woo, J. S. & Lee, E. H. Calsequestrin1 is an active partner of stromal interaction molecule 2 in skeletal muscle. *Cells* **10**, 2821. https://doi.org/10.3390/cells10112821 (2021).
27. Wang, L. et al. Retrograde regulation of STIM1-Orai1 interaction and store-operated Ca^{2+} entry by calsequestrin. *Sci. Rep.* **5**, 11349 (2015).
28. Wei, L., Hanna, A. D., Beard, N. A. & Dulhunty, A. F. Unique isoform-specific properties of calsequestrin in the heart and skeletal muscle. *Cell Calcium* **45**, 474–484. https://doi.org/10.1016/j.cerca.2009.03.006 (2009).
29. Zhang, L., Wang, L., Li, S., Xue, J. & Luo, D. Calsequestrin-1 regulates store-operated Ca^{2+} entry by inhibiting STIM1 aggregation. *Cell. Physiol. Biochem.* **38**, 2183–2193. https://doi.org/10.1159/000445574 (2016).
30. Lin, E. C. et al. Properties of WT and mutant hERG K(+) channels expressed in neonatal mouse cardiomyocytes. *Am. J. Physiol. Heart Circ. Physiol.* **298**(6), H1842-1849 (2010).
31. MedCalc Software Ltd. Comparison of means calculator. https://www.medcalc.org/calc/comparison_of_means.php (Version 23.1.7; Accessed 18 Feb 2025).

32. Olivera, J. F. & Pizarro, G. Two inhibitors of store operated Ca^{2+} entry suppress excitation contraction coupling in frog skeletal muscle. *J. Muscle Res. Cell Motil.* **31**, 127–139 (2010).
33. Stiber, J. et al. STIM1 signaling controls store-operated calcium entry required for development and contractile function in skeletal muscle. *Nat. Cell Biol.* **10**, 688–697 (2008).
34. Pitake, S. & Ochs, R. S. Membrane depolarization increases ryanodine sensitivity to Ca^{2+} release to the cytosol in L6 skeletal muscle cells: Implications for excitation–contraction coupling. *Exp. Biol. Med.* **241**(8), 854–862. https://doi.org/10.1177/1535370215619 (2015).
35. Bootman, M. D. et al. 2-aminoethoxydiphenyl borate (2-APB) is a reliable blocker of store-operated Ca^{2+} entry but an inconsistent inhibitor of InsP3-induced Ca^{2+} release. *FASEB J.* **16**(10), 1145–1150 (2002).
36. Rasmussen, H. B. et al. Subcellular localization of the delayed rectifier K^+ channels KCNQ1 and ERG1 in the rat heart. *Am. J. Physiol. Heart Circ. Physiol.* **286**, H13-139 (2004).
37. Sartori, R., Romanello, V. & Sandri, M. Mechanisms of muscle atrophy and hypertrophy: Implications in health and disease. *Nat. Commun.* **12**, 330. https://doi.org/10.1038/s41467-020-20123-1 (2021).
38. Jones, D. K. et al. hERG 1b is critical for human cardiac repolarization. *PNAS* **111**, 18073–18077. https://doi.org/10.1073/pnas.1414945111 (2014).
39. Nelson, B. R. et al. Skeletal muscle specific T-tubule protein STAC3 mediates voltage-induced Ca^{2+} release and contractility. *PNAS* **110**(29), 11881–11886. https://doi.org/10.1073/pnas.1310571110/-/DCSupplemental (2013).
40. Berbey, C. & Allard, B. Electrically silent divalent cation entries in resting and active voltage-controlled muscle fibers. *Biophys. J.* **96**, 2648–2657 (2009).
41. Perni, S., Close, M. & Franzini-Armstrong, C. Novel details of calsequestrin gel conformation in situ. *J. Biol. Chem.* **288**, 31358–31362 (2013).
42. Woo, J. S., Jeong, S. Y., Park, J. H., Choi, J. H. & Lee, E. H. Calsequestrin: A well-known but curious protein in skeletal muscle. *Exp. Mol. Med.* **52**, 1908–1925. https://doi.org/10.1038/s12276-020-00535-1 (2020).
43. Wang, Q. & Michalak, M. Calsequestrin, structure, function, and evolution. *Cell Calcium* **90**, 102242. https://doi.org/10.1016/j.ceca.2020.102242 (2020).
44. Beard, N. A. et al. Regulation of ryanodine receptors by calsequestrin: Effect of high luminal Ca^{2+} and phosphorylation. *Biophys. J.* **88**, 3444–3454 (2005).
45. Herzog, A., Szegedi, C., Jona, I., Herberg, F. W. & Varsanyi, M. Surface plasmon resonance studies prove the interaction of skeletal muscle sarcoplasmic reticular Ca^{2+} release channel/ryanodine receptor with calsequestrin. *FEBS Lett.* **472**, 73–77 (2000).
46. Beard, N. A., Sakowska, M. M., Dulhunty, A. F. & Laver, D. R. Calsequestrin is an inhibitor of skeletal muscle ryanodine receptor calcium release channels. *Biophys. J.* **82**, 310–320 (2002).
47. Cherednichenko, G. et al. Enhanced excitation-coupled calcium entry in myotubes expressing malignant hyperthermia mutation R163C is attenuated by dantrolene. *Mol. Pharmacol.* **73**, 1203–1212. https://doi.org/10.1124/mol.107.043299 (2008).
48. Gach, M. P. et al. Alpha2delta1 dihydropyridine receptor subunit is a critical element for excitation-coupled calcium entry but not for formation of tetrads in skeletal myotubes. *Biophys. J.* **94**, 3023–3034 (2008).
49. Mosca, B. et al. Enhanced dihydropyridine receptor calcium channel activity restores muscle strength in JP45/CASQ1 double knockout mice. *Nat. Comm.* **4**, 1541. https://doi.org/10.1038/ncomms2496 (2013).
50. Mosca, B. et al. Role of the JP45-calsequestrin complex on calcium entry in slow twitch skeletal muscles. *J. Biol. Chem.* **291**(28), 14555–14565 (2016).
51. Dainese, M. et al. Anesthetic- and heat-induced sudden death in calsequestrin-1-knockout mice. *FASEB* **23**, 1710–1720. https://doi.org/10.1096/fj.08-121335 (2009).
52. Protasi, F., Girolami, B., Serano, M., Pietrangelo, L. & Paolini, C. Ablation of calsequestrin-1 Ca^{2+} unbalance and susceptibility to heat stroke. *Front. Physiol.* **13**, 1033300. https://doi.org/10.3389/fphys.2022.1033300 (2022).
53. Boncompagni, S., Protasi, F. & Franzini-Armstrong, C. Sequential stages in the age dependent gradual formation and accumulation of tubular aggregates in fast twitch muscle fibers: SERCA and calsequestrin involvement. *Age (Dordr)* **34**(1), 27–41. https://doi.org/10.1007/s11357-001-9211-y (2012).
54. Boncompagni, S., Michelucci, A., Pietrangelo, L., Dirksen, R. T. & Protasi, F. Addendum: Exercise-dependent formation of new junctions that promote STIM1-Orai1 assembly in skeletal muscle. *Sci. Rep.* **8**(1), 17463. https://doi.org/10.1038/s41598-018-33063-0 (2018).
55. Michelli, A., Boncompagni, S., Pietrangelo, L., Takano, T. & Dirksen, R. T. Pre-assembled Ca^{2+} entry units and constitutively active Ca^{2+} entry in skeletal muscle of calsequestrin-1 knockout mice. *J. General Physiol.* **152**(10), e202012617. https://doi.org/10.1085/jgp.202012617 (2020).
56. Paolini, C. et al. Reorganized stores and impaired calcium handling in skeletal muscle of mice lacking calsequestrin-1. *J. Physiol.* **583**(Pt 2), 767–784. https://doi.org/10.1113/jphysiol.2007.138024 (2007).
57. Smith, L. R. & Meyer, G. A. Skeletal muscle explants: Ex-vivo models to study cellular behavior in a complex tissue environment. *Connect. Tissue Res.* **61**(3–4), 248–261 (2020).
58. Gillies, A. R. & Lieber, R. L. Structure and function of the skeletal muscle extracellular matrix. *Muscle Nerve* **44**(3), 318–331. https://doi.org/10.1002/mus.22094 (2011).
59. Goswami, A. et al. Accumulation of STIM1 is associated with the degenerative muscle fibre phenotype in ALS and other neurogenic atrophies. *Neuropath. Appl. Neurobiol.* **41**, 304–318 (2015).
60. Lopez, J. R., Kaura, V., Diggle, C. P., Hopkins, P. M. & Allen, P. D. Malignant hyperthermia, environmentl heat stress, and intracellular calcium dysregulation in a mouse model expressing the p.G2435R variant of RyR1. *Brit. J. Anaesth.* **121**(4), 953–961. https://doi.org/10.1016/j.bja.2018.07.008 (2018).
61. Perez-Neut, M., Shum, A., Cuvas, B. D., Miller, R. & Gentile, S. Stimulation of hERG1 channel activity promotes a calcium-dependent degradation of cyclin E2, but not cyclin E1, in breast cancer cells. *Oncotarget* **6**, 1631–1639 (2015).
62. Pond, A. L., Petrecca, K., Van Wagoner, D. R., Shrier, A. & Nerbonne, J. M. Expression of distinct ERG proteins in rat, mouse and human heart: Relation to functional I_{Kr} channels. *J. Biol. Chem.* **275**, 5997–6006 (2000).
63. Brawek, B. & Garaschuk, O. Network-wide dysregulation of calcium homeostasis in Alzheimer's disease. *Cell Tissue Res.* **357**, 427–438 (2014).
64. Cheng, A. J., Andersson, D. C. & Lanner, J. T. Can't live with or without it: Calcium and its role in Duchenne muscular dystrophy-induced muscle weakness. *Am. J. Physiol. Cell Physiol.* **308**, C697–C698 (2015).
65. Sama, D. M. & Norris, C. M. Calcium dysregulation and neuroinflammation: Discrete and integrated mechanisms for age-related synaptic dysfunction. *Ageing Res. Rev.* **12**, 982–995 (2013).
66. Wang, Y. et al. Uncoupling of Cav1.2 from Ca^{2+}-induced Ca^{2+} release and SK channel regulation in pancreatic β-cells. *Mol. Endocrinol.* **28**, 458–476 (2014).
67. Babcock, JJ, Li M. hERG channel function: beyond long QT. Acta Pharmacologic Sinica **34**, 329–335. https://doi.org/10.1038/aps.2013.6 (2013).
68. Bannister, RA, Beam, KG. Cav1.1: The atypical prototypical voltage-gated Ca2+ channel. Biochimica et BiophysicaActa **1828**, 1587–1597 (2013).
69. Bilmen JG, Michelangeli F. Inhibition of the type 1 inositol 1,4,5-triphosphat receptor by 2-aminoethoxydiphenylborate. *Cellular Signalling* **14**, 955–960 (2002).

70. Paolini, C., Quarta, M., Wei-LaPierre, L., Michelucci, A., Nori, A., Reggiani, C., Dirksen, R. T., Protasi, F. Oxidative stress,mitochondrial damage, and cores in muscle from calsequetrin-1 knockout mice. *Skeletal Muscle* **5**, 10.https://doi.org/10.1186/s13395-015-0035-9 (2015).
71. Pond AL, Nedele C, Wang WH, Wang X, Walther C, Jaeger C, et al. The mERG1a channel modulates skeletal muscleMuRF1, but not MAFbx, expression. *Muscle Nerve*. **49**, 378–88 (2014).

Author contributions

A.L.P. is the corresponding author and is responsible for handling of the manuscript. G.H.H. and A.L.P. conceived and designed the project; acquired, analyzed, and interpreted data for some data sets, also designing figures for these data sets; guided the students who gathered data; co-wrote the initial manuscript and revised the manuscript per co-author suggestions. S.Z. contributed expertise for immunoblot work and to interpretation of these data sets; contributed strongly to development of the discussion; carefully reviewed and edited all versions of the manuscript. J.K. developed the statistical programs for intracellular calcium concentration assays (fura-2 analyses) and aided in drawing statistical conclusions; carefully reviewed and edited the initial and all later versions of the manuscript for statistical accuracy. W.H.W. cloned the cassette for development of the HERG-encoded adenovirus and aided with development of the method used to transduce the myotubes for HERG overexpression; and reviewed the final manuscript. E.P., S.G., E.L., and C.W. are/were graduate students who performed various studies, analyzed the data (with guidance of J.K., A.L.P., or G.H.H.), interpreted that data, and developed subsequent figures; they carefully reviewed the final versions of the manuscript. S.G. reviewed all versions of the manuscript and contributed strongly to its final version. N.M. is a SIU medical student who cultured cells and performed fura assays for RyR1 and SOCE activities; she analyzed and interpreted her data (with guidance) and contributed this to development of Figs. 6 and 7. O.K. was an undergraduate student who cultured cells and performed fura-2 assays for ECCE; he analyzed and interpreted the data (with guidance) which contributed to development of some parts of figures.

Funding

The research reported in this publication was supported in large part by the Department of Defense office of the Congressionally Directed Medical Research Programs through a Peer Reviewed Medical Research Program (PRMRP) Discovery Award to ALP and GHH. The Southern Illinois University Carbondale (SIUC) Graduate School provided some financial support through funding to graduate students CW and SG. SIUC also provided some support through an Undergraduate Research-Enriched Academic Challenge (REACH) Award to OK. The Southern Illinois School of Medicine provided some financial support through their Medicine Mentor Professional Enrichment Experience Program to NM.

Declarations

Competing interests

The authors declare no competing interests.

Additional information

Supplementary Information The online version contains supplementary material available at https://doi.org/10.1038/s41598-025-93788-7.

Correspondence and requests for materials should be addressed to A.L.P.

Reprints and permissions information is available at www.nature.com/reprints.

Publisher's note Springer Nature remains neutral with regard to jurisdictional claims in published maps and institutional affiliations.